414

A Thesis
entitled

MEASUREMENT OF THE INNER POTENTIALS OF CRYSTALS

by

Aparna Goswami, M.Sc.

Submitted for the
Degree of Master of Philosophy
of the
University of London

Imperial College of Science and Technology
London

1978

ABSTRACT

It is predicted on theoretical grounds that within a crystalline solid there is a positive potential of the order of 10 volts. This potential - the "inner potential" - is responsible for a refraction effect on electrons interacting with the crystal and use is made of this to measure its value experimentally.

In the present work, the combined effect of refraction and diffraction on a beam of high energy electrons (in the range 40 to 50 kV) has been used to obtain values for the inner potential of copper, silver, gold and diamond, the experiments being carried out in a vertical electron diffraction camera.

For the metals mentioned suitably flat (111) crystalline surfaces were formed by deposition, in vacuum, on the cleavage faces of mica and of magnesium oxide. The measurements of the inner potential of these metals gave 13.4 $\pm$ 0.8 volts, 17.7 $\pm$ 0.9 volts, and 21.4 $\pm$ 1.1 volts respectively. The values quoted are based on many individual measurements from several specimens of each metal. In the case of diamond, only three specimens were available, one with a natural (111) face, the other two having artificially polished faces. The inner potential value was based on many individual measurements on each diamond, this being about 14 or 15 volts depending on the specimen used. One of these was a "type II" or "conducting" diamond and was used to determine whether or not the effects of (the possible) electrostatic charging of the other two (non-conducting) diamonds influenced the measured inner potential. Within the estimated experimental errors, no significant difference was found.

The values of the inner potential for the above substances agree fairly well with recent theoretical calculations but differ considerably from those of some past experimental work.

CONTENTS

		Page
	ABSTRACT	2
Chapter 1	INTRODUCTION	6
Chapter 2	METHODS USED TO MEASURE INNER POTENTIAL	14
2.1	General	14
2.2	Yamaguti's method	14
2.3	Shinohara's method	23
Chapter 3	APPARATUS USED IN PRESENT WORK	30
Chapter 4	EXPERIMENTAL PROCEDURE	32
4.1	Preparation of the specimens - general	32
4.1.1	Preparation of copper, silver and gold specimens	32
4.1.2	Specimens of diamond	32
4.1.3	Specimens of sodium chloride, potassium bromide and calcium fluoride	34
4.1.4	Mounting of specimens	34
4.2	Photographic recording - general	34
4.2.1	Recording of Bragg spots	34
4.2.2	Recording of horizontal Kikuchi lines	38
4.3	Measurements - general	38
4.3.1	Treatment of the readings	40
4.3.2	(a) Typical calculation for a Yamaguti type experiment on gold	41
	(b) Typical calculation for a Shinohara type experiment on diamond	44
Chapter 5	EXPERIMENTAL RESULTS	46
5.1	General	46
5.2	Note on camera length	46
5.3	Note on electron beam energy	46
5.4	Presentation of the results	48
5.5	Copper	48
5.6	Silver	49
5.7	Gold	52

Page

5.8 Diamond 53

5.9 Summary of the results for copper, silver, gold and diamond 59

5.10 Results for sodium chloride, potassium bromide, calcium fluoride and silicon 60

Chapter 6 THE THEORETICAL CALCULATION OF INNER POTENTIAL 61

6.1 General 61

6.2 The method of Shinohara and Miyake 62

6.3 An approximation for the atomic scattering factors 64

6.4 A simplified method for evaluation of inner potential 72

6.5 Calculations using recent Hartree-Fock wave functions 74

6.6 The calculated values for sodium chloride, potassium bromide, calcium fluoride and silicon 75

Chapter 7 SUMMARY AND COMMENTS 77

7.1 General 77

7.2 Experimental 77

7.2.1 Silver and gold 77

7.2.2 Copper 79

7.2.3 Diamond 80

7.3 Comments on the theoretical calculations 81

Appendix 1: Relation between the inner potential $\bar{\Phi}$ and the refractive index μ of a crystal. 84

Appendix 2: Wavelength and camera length consideration. 85

Appendix 3: Yoshida's (1954) method for measuring inner potential. 90

ACKNOWLEDGEMENTS 92

REFERENCES 93

CHAPTER 1

INTRODUCTION

A crystal consists of a regular array of atoms, each comprising a positive nucleus surrounded by a "cloud" of negatively charged electrons. This regular three-dimensional distribution of charges gives rise to a positive electrostatic potential, having the periodicity of the crystal lattice. The volume average of the periodic potential inside a crystal is constant and is known as the "inner potential" ($\bar{\phi}$) of the crystal.

The existence of such a potential was first postulated by Bethe (1927, 1928a). Davisson and Germer (1927) studied the diffraction of electrons by a single crystal of nickel, but were unable to correlate the diffracted beam with the known structure of the crystal. Bethe showed that this problem could be satisfactorily resolved by assuming that there was a positive potential of about 15 volts inside the crystal. Since then many investigations, both theoretical and experimental, have been carried out on inner potential (see, for example, Thomson and Cochrane 1939, and Pinsker 1951).

Due to the presence of the inner potential, an electron beam entering or leaving a crystal surface will experience, in general, a refraction effect and from the observations of the positions of Bragg diffraction spots or Kikuchi patterns the refractive index can be deduced. (The early measurements of inner potential for a number of substances were carried out using slow electrons, but because of the theoretical difficulties encountered in interpreting the experimental observations, the results are

regarded, in the main, as unreliable and will not be further considered here.) It was soon realized that fast electrons should be suitable for measuring inner potential and many such measurements were made during the first two decades after the discovery of electron diffraction, particularly by Yamaguti (1930, 1932) and Shinohara (1932a). Yamaguti's method depends on the observation of the effect of refraction on Bragg diffraction spots and Shinohara devised another method based on the refraction of Kikuchi patterns (see Chapter 2, Sections 2.2 and 2.3). The above methods have been applied to a variety of crystals, for example, alkali halides, mica, diamond, calcite, quartz, zincblende, etc. These substances were chosen, generally, because they could be cleaved easily, thus producing atomically flat surfaces. Such surfaces are necessary for the application of Yamaguti and Shinohara's method to the measurement of inner potential.

A third method employing fast electrons, which can be used in conjunction with polycrystalline specimens, has been devised by Mollenstedt and Duker (1956). It is based on an electron interference effect and is analogous to the optical Fresnel biprism interferometer. The electron biprism consists of a quartz fibre about 1 μm diameter coated with gold to make it electrically conducting. The fibre is mounted midway between two earthed metal plates about 5 mm long and 4 mm apart. If the potential of the fibre is a few volts positive to earth, electrons passing near it are deviated through an angle which is independent of the perpendicular distance of the electron trajectory from the fibre (see Fig. 1.1). Briefly, the measurement of inner potential is carried out as follows. A thin film of a given material, having a sharp boundary

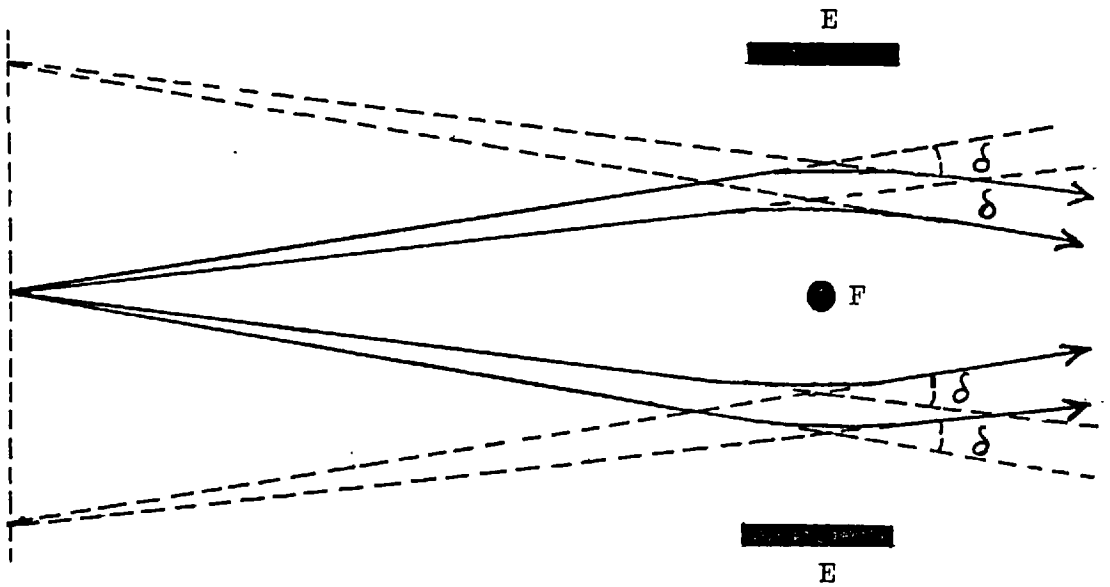


FIG. 1.1 Mollenstedt biprism.

F - Gold coated quartz fibre, 1 μm diameter.
E - Earthed metal plates.

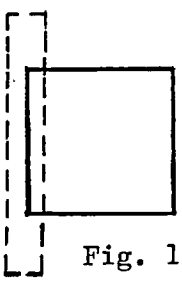


Fig. 1.2(a)

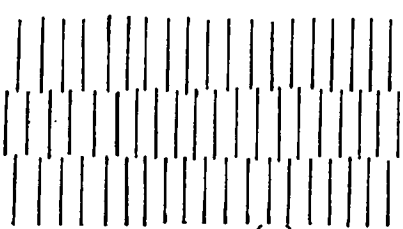


Fig. 1.2(b)

FIG. 1.2(a) shows the object, indicated by a solid outline, on which is superimposed a broken outline representing the shadow of the biprism in the object plane.

FIG. 1.2(b) represents the general appearance of interference micrographs obtained with a Mollenstedt interferometer.

between two regions of different thickness, is mounted below the biprism (see Fig. 1.2a). The interference pattern, consisting of one set of parallel fringes displaced with respect to another set (see Fig. 1.2b) is recorded photographically. If n is the displacement measured in terms of the fringe spacing as a unit, t the film thickness difference and μ the refractive index for the electrons, then it can be shown that $n = (\mu - 1)t/\lambda$, where λ is the electron wavelength. (λ can also be measured with sufficient accuracy using the biprism device.) From μ, $\bar{0}$, the inner potential, can be deduced. (For a detailed description, see, for example, Rymer 1970.)

The present work is concerned primarily with measuring the inner potentials of copper, silver, gold and diamond using fast electrons and for this reason, the following review of past measurements and calculations will be confined to these four substances.

a) Diamond

Using both Yamaguti's and Shinohara's method, Beeching (1935) obtained a value of 20.8 $\pm$ 0.7 volts for the inner potential of diamond. Hartmann, Neimitz and Schwarzer (1975) using a modified method for the experimental evaluation of inner potential from Kikuchi patterns obtained 18.6 $\pm$ 2.2 volts.

Miyake (1940) calculated the mean inner potential of diamond from considerations of the diamagnetic susceptibility to be in the range 11.3 to 18.3 volts and Radi (1970) using the most recent Hartree-Fock-Slater atomic radial functions obtained 15.9 volts.

b) Copper, silver and gold

Using Yamaguti's method, Tull (1951a) measured the inner potential of silver and gold to be 23.3 ± 1.0 volts and 30.2 ± 0.9 respectively. High energy electron diffraction from electropolished surfaces of copper and silver were investigated by Yoshida (1954) who obtained 8 to 14 volts and 22 ± 6 volts respectively. Using the electron interferometric method, Buhl (1959) obtained for silver and gold 20.7 ± 0.7 volts and 21.2 ± 2 volts respectively and Keller (1961) found for copper, silver and gold 23.5 ± 0.6 volts, 17.0 to 21.8 volts and 22.1 to 27 volts respectively. Hoffmann and Jonson (1965) obtained 20 volts for copper. A later interferometric measurement, using improved apparatus, made by Kerschbaumer (1967) on copper and gold gave 20.2 ± 0.7 volts and 16.8 ± 1.0 volts respectively. High energy electron diffraction patterns were taken from electropolished surfaces of copper by Steeb and Bühner (1967a) in reflection and displacements of the diffraction spots from the Bragg positions in the absence of the refraction effect were observed. From these measurements a value of 19 volts was obtained.

The results are summarized in Table 1.1 overleaf.

Theoretical calculations for the inner potential of copper, silver, gold and diamond have been made by different workers and these are summarized in the following table, Table 1.2.

A few of the above mentioned methods used for the calculation of inner potential will be considered in Chapters 6 and 7.

It is evident from the foregoing that there are discrepancies within both the past experimental and theoretical values for the inner

Experimental	ϕ in volts				Method used
	Cu	Ag	Au	Diamond	
1) Beeching (1935)	-	-	-	20.8 ± 0.7	Reflection (Yamaguti)
2) Tull (1951a)	-	23.3 ± 1.0	$30.2 \pm .9$	-	Reflection (Yamaguti)
3) Yoshida (1954)	8 to 14	22 ± 6	-	-	Reflection.
4) Buhl (1959)	-	20.7 ± 0.7	21.2 ± 2.0	-	Electron biprism interferometer.
5) Keller (1961)	$23.5 \pm .6$	17. to 21.8	22.1 to 27	-	Electron biprism interferometer.
6) Hoffmann and Jonson (1965)	20.0	-	-	-	Electron biprism interferometer.
7) E. Kerschbaumer (1967)	$20.2 \pm .7$	-	16.8 ± 1.0	-	Electron biprism interferometer.
8) Steeb and Bühner (1967)	19.0	-	-	-	Reflection measurements (Yamaguti).
9) Schwarzer et al (1975)	-	-	-	18.6 ± 2.2	Reflection. From Kikuchi pattern (Shinohara).

TABLE 1.1

Theoretical	Φ in volts for				Method used
	Copper	Silver	Gold	Diamond	
1) Veldkamp, J. (1933)	16.9	-	-	-	
2) Miyako (1940)	-	-	-	11.3 to 18.3	From considerations of diamagnetic susceptibility.
3) Tull (1951b)	13.7	22.1	35.9	-	From exponential approximation of scattering factor and using Pauling's function.
4) Siota, Y. (1958)	20.2	21.8	30.0	13.7	Using Hartree (1932) distribution and wave function by Fucho (1935).
5) Anishchenkov (1966)	a) 20.8 b) 23.4	21.7 -	30.1 33.5	-	Thomas Fermi Dirac and Thomas Fermi statistics.
6) Steeb and Bühner (1967b)	18.43	-	-	-	Using analytic approximations to X-ray scattering factors.
7) Radi (1970) "low" "high"	15.8 19.98	18.7 21.87	25.0 28.2	15.9 19.75	Using recent Hartree-Fock-Slater wave function.

TABLE 1.2

potential of the above (and other) substances, and the present work has been carried out in an attempt to resolve at least some of the differences.

CHAPTER 2

METHODS USED TO MEASURE INNER POTENTIAL

2.1 GENERAL

Measurements were carried out on several different crystals, using an electrom beam of about 45 kV energy, in a vertical electron diffraction camera (see Chapter 3, and Kehoe, 1956). In all cases the incident beam was allowed to make small glancing angles with a flat surface of each crystal. The diffracted electrons were associated with crystal planes parallel to the flat surface. Two methods based on the above "reflection" technique were used, one due to Yamaguti (1930, 1932) and the other to Shinohara (1932). These will be described in detail in the following two sections.

2.2 YAMAGUTI METHOD

The refractive index μ due to the inner potential $\bar{\Phi}$ is defined by the relation:

$$\mu^2 = 1 + \frac{\bar{\Phi}}{P} = \frac{\lambda_o^2}{\lambda_i^2} \qquad \text{(see Appendix 1)} \qquad (2.1)$$

where P is the electron accelerating potential, λ_o the electron wavelength in vacuum and λ_i the corresponding wavelength inside the crystal.

In the absence of the inner potential, the various orders of diffraction would be given by the Bragg equation:

$$2d_{hkl} \operatorname{Sin} \theta_n = n\lambda_o \qquad (2.2)$$

where d_{hkl} is the spacing of the planes parallel to the surface of the crystal, θ_n is the glancing angle (the Bragg angle) which the beam makes with the crystal surface, and n is the diffraction order number (see Fig. 2.1).

In the presence of the inner potential, the incident and diffracted beam will experience a refraction effect, the incident beam on entering the crystal and diffracted beam on leaving the crystal (see Fig. 2.2). It is evident that the grazing angle β_n will be somewhat less than the Bragg angle θ_n - now associated with wavelength λ_i.

From Snell's law:

$$\frac{\text{Cos } \beta_n}{\text{Cos } \theta_n} = \mu \quad \text{or} \quad \mu^2 = \frac{1 - \sin^2 \beta_n}{1 - \sin^2 \theta_n} = \frac{\lambda_o^2}{\lambda_i^2} \tag{2.3}$$

Rearranging, equation (2.3) gives:

$$\mu^2 - 1 = \mu^2 \sin^2 \theta_n - \sin^2 \beta_n$$

$$= \frac{\lambda_o^2}{\lambda_i^2} \sin^2 \theta_n - \sin^2 \beta_n$$

and using equation (2.2):

$$\mu^2 - 1 = \frac{n^2 \lambda_o^2}{4 d_{hkl}^2} - \sin^2 \beta_n \tag{2.4}$$

It is evident that equation (2.4) can be used in general with any Bragg reflection to obtain μ, provided d_{hkl}, β_n and λ_o are known. Of these quantities, d_{hkl} will be known accurately from X-ray crystallographic data and β_n can be measured from a photographic record of the sequence of Bragg spots produced as the angle

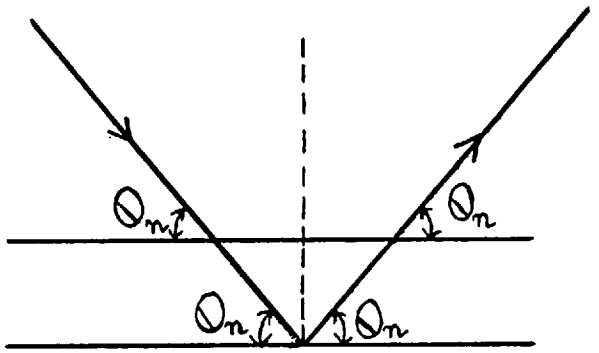

θ_n
θ_n
θ_n
θ_n

FIG. 2.1

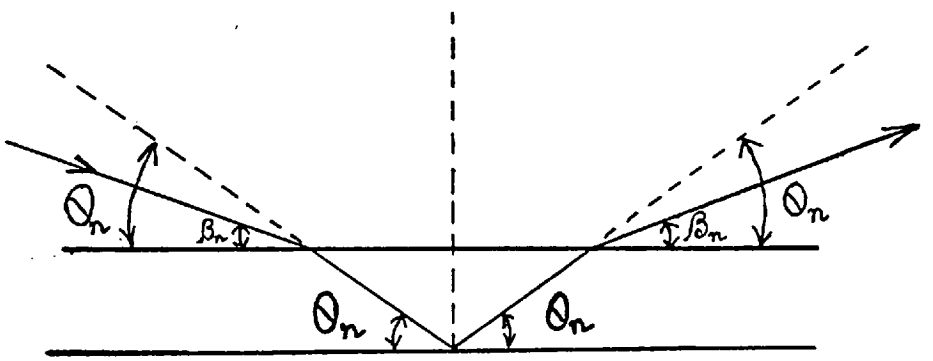

θ_n
β_n
β_n
θ_n
θ_n
θ_n

FIG. 2.2

of grazing incidence is changed (see Fig. 2.3). Thus:

$$\beta_n = \tfrac{1}{2} \tan^{-1} \frac{r_n^*}{L} \qquad (2.5)$$

Both r_n^*, the distance from the point where the undeflected beam strikes the photographic plate to the n^{th} Bragg diffraction spot and L, the camera length, i.e. the distance between the photographic plate and the specimen, can be measured with sufficient accuracy. Unfortunately, the direct accurate measurement of λ_o presents a major difficulty and without very sophisticated potential measuring apparatus it can only be determined roughly by using a not-very-accurate meter on the E.H.T. supply to the camera.

Yamaguti avoided this difficulty by the following procedure. Using a rough value of the wavelength, λ_o' (deduced for example from the E.H.T. supply voltmeter), a quantity (μ_n^2-1) can be obtained for the different Bragg angles by measuring β_n [see equation (2.5) - thus obtaining $\sin^2\beta_n$] and calculating the quantity $n^2\lambda_o'^2/4d_{hkl}^2$. Thus:

$$\mu_n^2 - 1 = \frac{n^2\lambda_o'^2}{4d_{hkl}^2} - \sin^2\beta_n \qquad (2.6)$$

so that $(\mu_n^2 - 1)$ will now vary with the order number n. Combining equation (2.4) with equation (2.6) gives:

$$\mu_n^2-1 = \frac{(\lambda_o'^2 - \lambda_o^2)}{4d_{hkl}^2} \cdot n^2 + (\mu^2 - 1) \qquad (2.7)$$

In equation (2.7), the quantities $(\mu_n^2 - 1)$ and n^2 are variables, the remaining terms $\lambda_o'^2$, λ_o^2, d_{hkl}^2 and $(\mu^2 - 1)$ all being constants. Hence if $(\mu_n^2 - 1)$ obtained from equation (2.6)

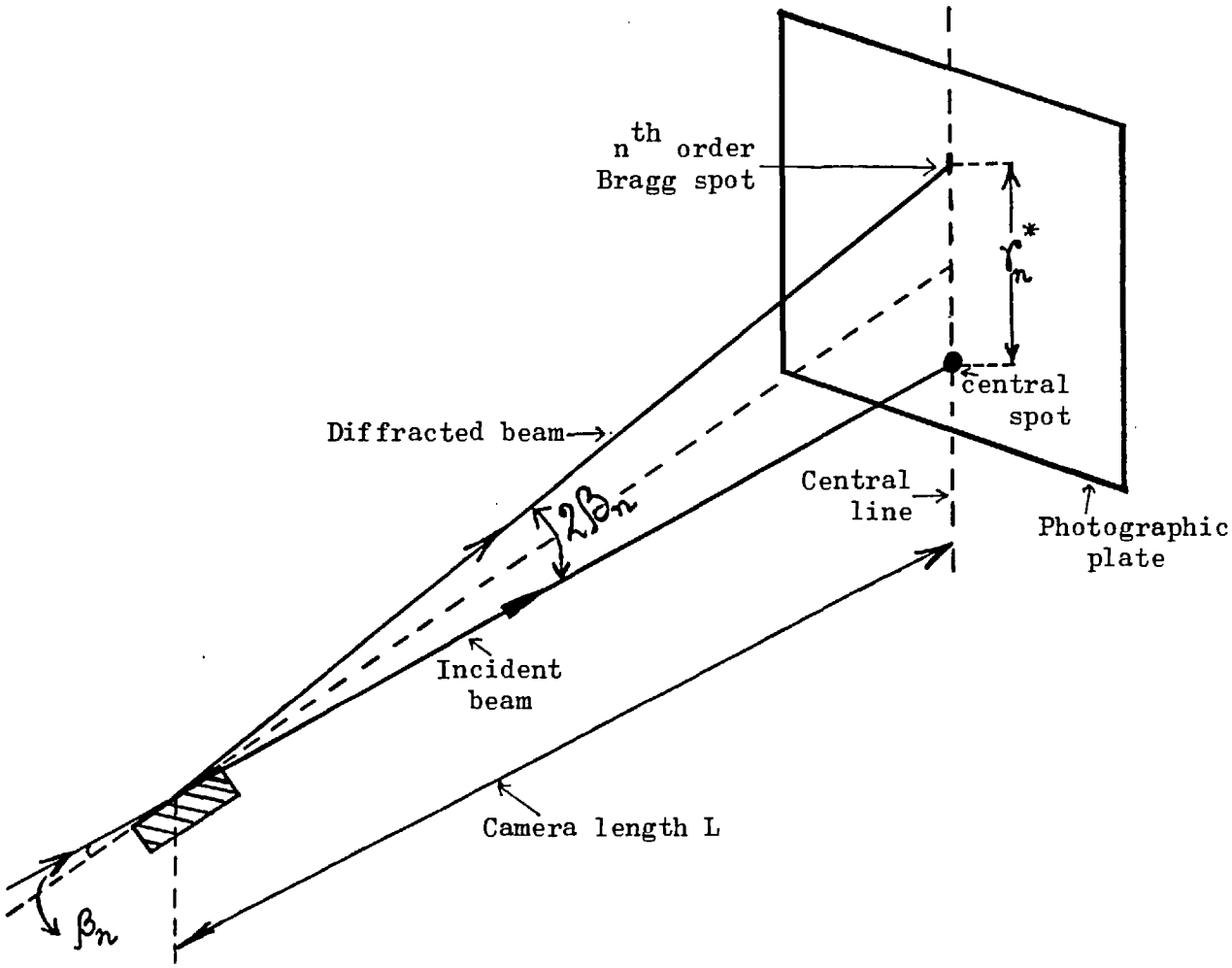

n^th order
Bragg spot
r*n
central
spot
Diffracted beam
2βn
Central
line
Photographic
plate
Incident
beam
Camera length L
βn

FIG. 2.3

is plotted against n^2, a straight line should result (see Fig. 2.4). The slope of the line will evidently lead to an accurate value of λ_o, and the intercept will give the value of $(\mu^2 - 1)$.

Finally, allowing for relativistic effects, the expression for the inner potential can be formed (see Yamaguti 1930). Thus:

$$\Phi = \frac{(\mu^2-1)h^2}{2em_o\lambda_o^2}\left(1 + \frac{h^2}{m_o^2c^2} \cdot \frac{1}{\lambda_o^2}\right)^{-\frac{1}{2}} \qquad (2.8)$$

where h is Planck's constant, e the electron charge, m_o the electron rest mass, and c the velocity of light in vacuum.

The positions of the Bragg reflections from which the values of β_n were calculated [see Fig. 2.3 and equation (2.5)] were obtained in two ways, viz.

(i) continuous changing of the angle of incidence while exposing the photographic plate so that the sequence of Bragg spots was obtained during the exposure (see Fig. 2.5). This is called the "rotation method".

(ii) setting the angle of incidence for each Bragg maximum and exposing the plate for each setting (see Fig. 2.6). This is called the "individual setting" method.

The "rotation" method has the advantage of requiring only a single exposure of the plate, during which all the Bragg spots are recorded, but because of the continuous motion of the specimen during exposure the diffraction spots tend to become elongated, especially the lower orders. The elongation leads to uncertainty in deciding the exact positions of the diffraction spot maximum.

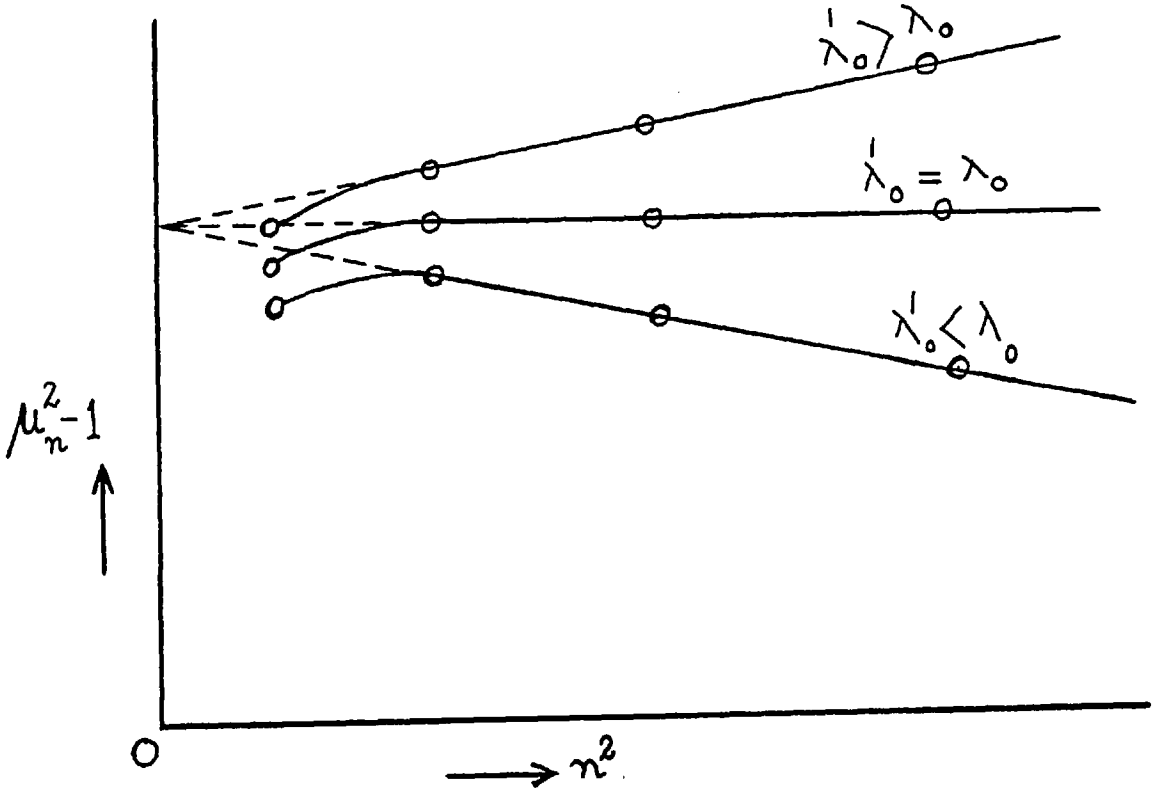


FIG. 2.4

(Note : the lowest values of $\mu_n^2 - 1$ tend to deviate from the straight lines because of low electron beam penetration and measuring difficulties associated with the often indistinct character of the low order diffraction spots)

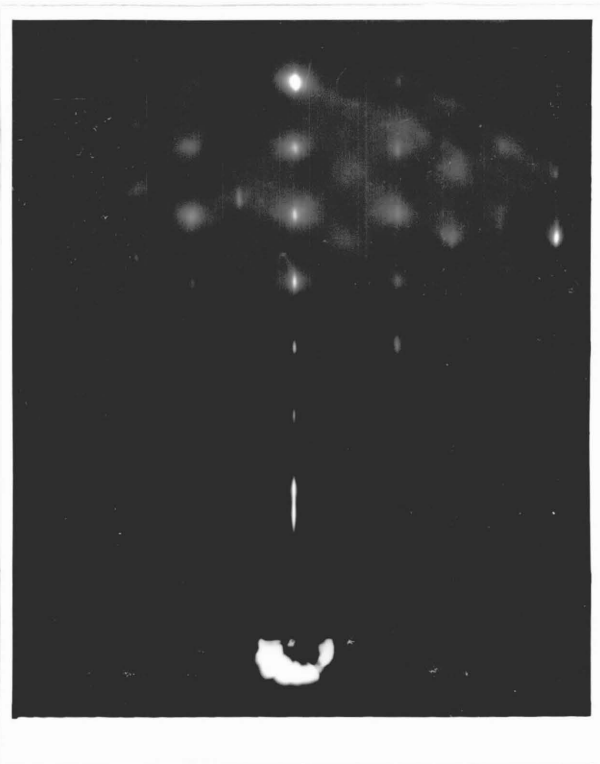


FIG. 2.5

'Rotation' photograph from silver (111) face



FIG. 2.6

"Individual setting" photograph
from Diamond (111) face

Another drawback is that the weak diffracted spots are sometimes not recorded because of insufficient exposure. The "individual setting" method overcomes the difficulty of recording weak diffractions since the exposure at each setting can be varied according to the strength of diffraction as judged by its appearance on the fluorescent screen before making the exposure. There is also less difficulty in assessing the centres of the diffraction spots because they are not elongated. The main disadvantage of the "individual setting" method results from setting errors, the actual setting being made when the spot is judged to be at its highest intensity. There is always a degree of uncertainty attached to these judgements.

2.3 SHINOHARA METHOD

This is based on the effect of refraction of electrons on the positions of Kikuchi lines, in the present instance of "horizontal" Kikuchi lines, associated with the crystal planes parallel to the flat surface of the crystal (see Figs. 2.7a and 2.7b). The geometry of these lines can be explained by supposing that, inside the crystal, inelastically scattered electrons, making the Bragg angle θ_n with the planes parallel to the surface, emerge from the crystal making an angle β_n with the surface. The emergent electrons then arrive at the fluorescent screen or photographic plate to form part of a "horizontal" Kikuchi line. (The lines are in fact slightly curved.) Because of the refraction effect due to the inner potential, β_n will be (as in the previous method) slightly less than θ_n and, as before, equation (2.4) will hold, i.e.

$$\mu^2 - 1 = \frac{n^2\lambda_o^2}{4d_{hkl}^2} - \sin^2\beta_n$$

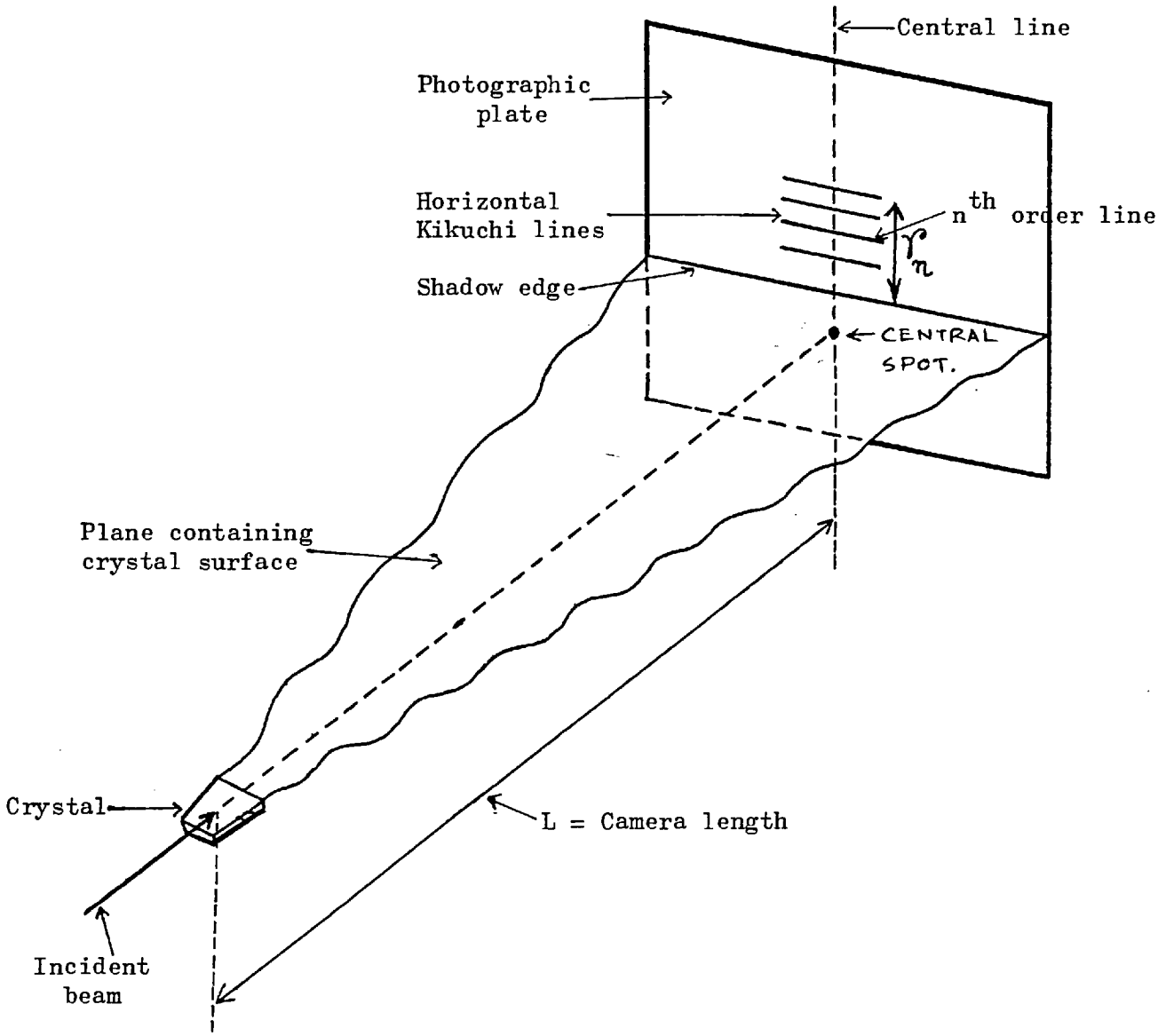

Central line
Photographic plate
Horizontal Kikuchi lines
n^th order line
r_n
Shadow edge
CENTRAL SPOT.
Plane containing crystal surface
Crystal
L = Camera length
Incident beam

FIG. 2.7(a)

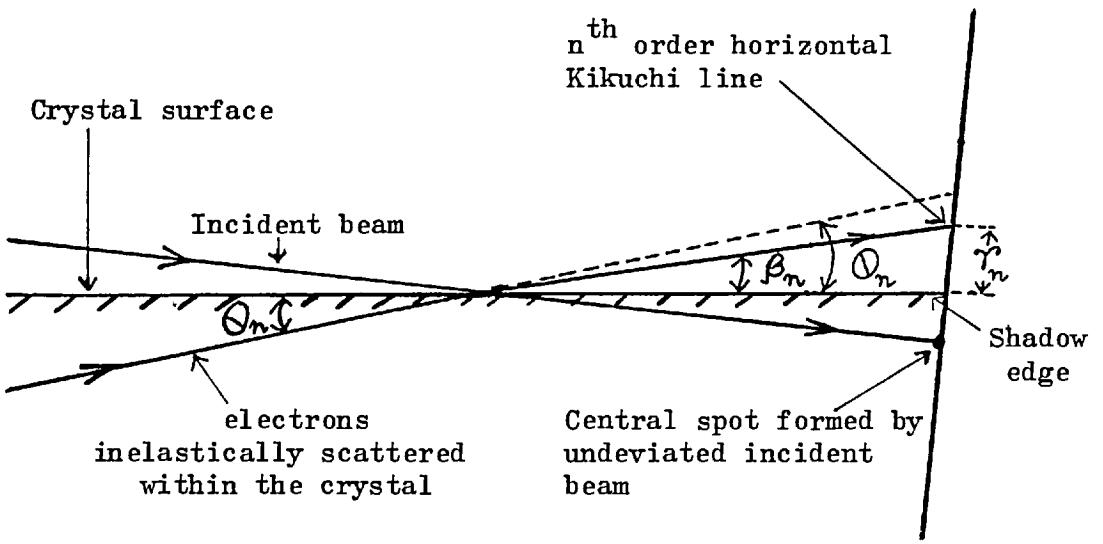

n^th order horizontal
Kikuchi line
Crystal surface
Incident beam
β_n
θ_n
γ_n
θ_n
Shadow
edge
electrons
inelastically scattered
within the crystal
Central spot formed by
undeviated incident
beam

FIG. 2.7(b)

and hence also equation (2.7), i.e.

$$\mu_n^2 - 1 = \frac{(\lambda'^2_o - \lambda_o^2)}{4d^2_{hkl}} .n^2 + (\mu^2 - 1)$$

The procedure then follows the Yamaguti method.

The special feature of the Shinohara method is that a single exposure of the plate is sufficient to record simultaneously several horizontal lines (see Fig. 2.8). The angle β_n is measured between the emergent n^{th} order diffraction direction and the plane containing the crystal surface. In practice, this is done by measuring the camera length L and the distance r_n along the central line on the photographic plate (see Fig. 2.7a), i.e. the distance between the n^{th} order Kikuchi line and the shadow edge. Thus (noting that r_n is much less than L):

$$\beta_n \simeq \tan^{-1} \frac{r_n}{L} \qquad (2.9)$$

Usually the shadow edge is not very distinct and to obtain a more accurate determination of β_n, the following procedure is adopted.

When the glancing angle between the incident beam and the crystal surface is varied, the Kikuchi pattern and the shadow edge move together to follow the change in the glancing angle. It is then possible to adjust the position of the pattern so as to bring the m^{th} Bragg spot on the central line (see Fig. 2.7a) into coincidence with the corresponding "horizontal" Kikuchi line (see Fig. 2.9). It then follows that for the n^{th} order Kikuchi line, the required angle β_n will be given by:

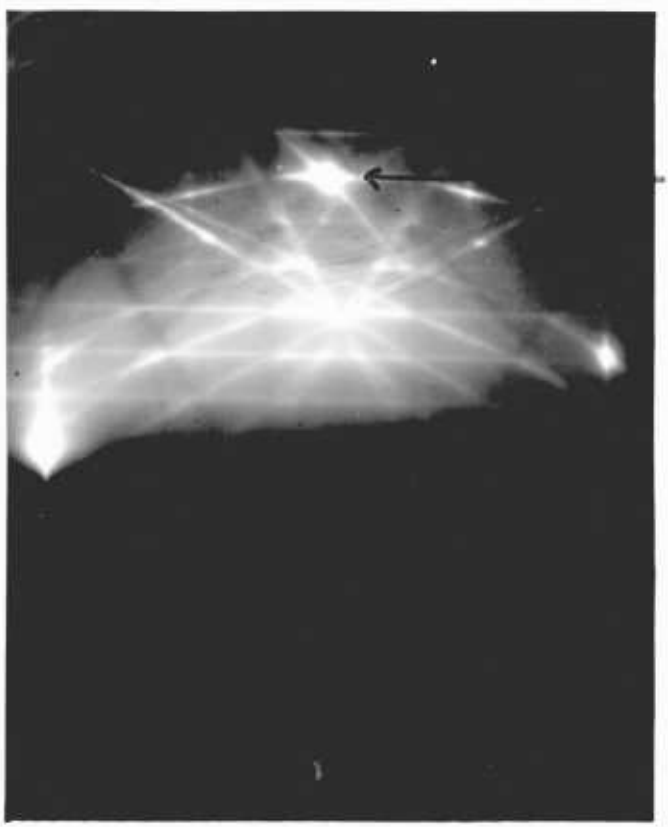


FIG. 2.8

Horizontal Kikuchi lines showing Bragg spot coincident with the corresponding line.

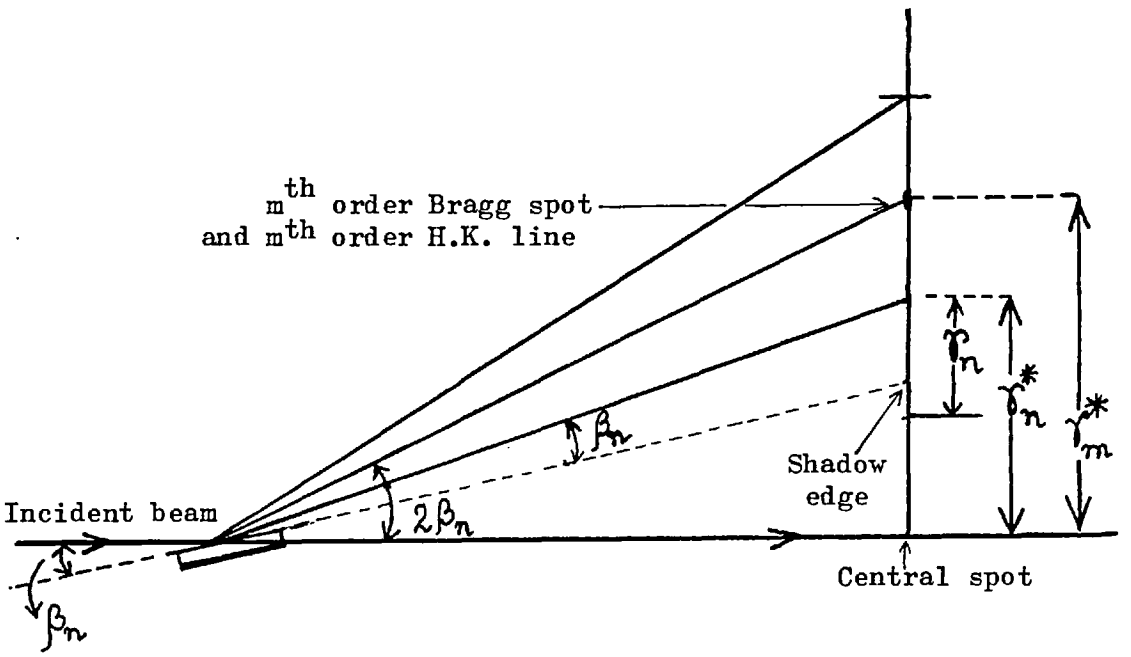

m th order Bragg spot
and m th order H.K. line
Incident beam
Shadow
edge
Central spot

FIG. 2.9

$$\beta_n = \tan^{-1} \frac{r_n^*}{L} - \tfrac{1}{2} \tan^{-1} \frac{r_m^*}{L} \qquad (2.10)$$

Equation (2.10) is used instead of (2.9) for determination of β_n and from here on the procedure is the same as that for the Yamaguti method described in Section 2.2, equation (2.8) being used to obtain ϕ.

CHAPTER 3

APPARATUS USED IN THE PRESENT WORK

All the experiments of the present work were carried out in a vertical electron diffraction camera designed by Kehoe, Newman and Pashley (see, for example, Kehoe 1956).

The operational details for the camera are as follows:

a) Maximum accelerating voltage about 60 kV.

b) Residual pressure about 10^{-5} torr.

c) Either Ilford N50 or Agfa Gevaert Scientia plates were used for the photographic recording of the diffraction patterns.

The specimen holder is shown diagrammatically in Fig. 3.1. The specimen can be tilted with respect to the beam (angle of incidence), i.e. rotated about the axis YY, and rotated azimuthally, i.e. about the axis XX. The specimen can be translated in either direction along XX. The surface of the specimen can also be scanned to some extent by the electron beam by tilting slightly the axis of the focussing coil.

Thin film single crystal specimens of silver etc. were formed in a vacuum deposition apparatus at a residual gas pressure of about 10^{-6} torr. (See also Chapter 4, Section 4.1.1).

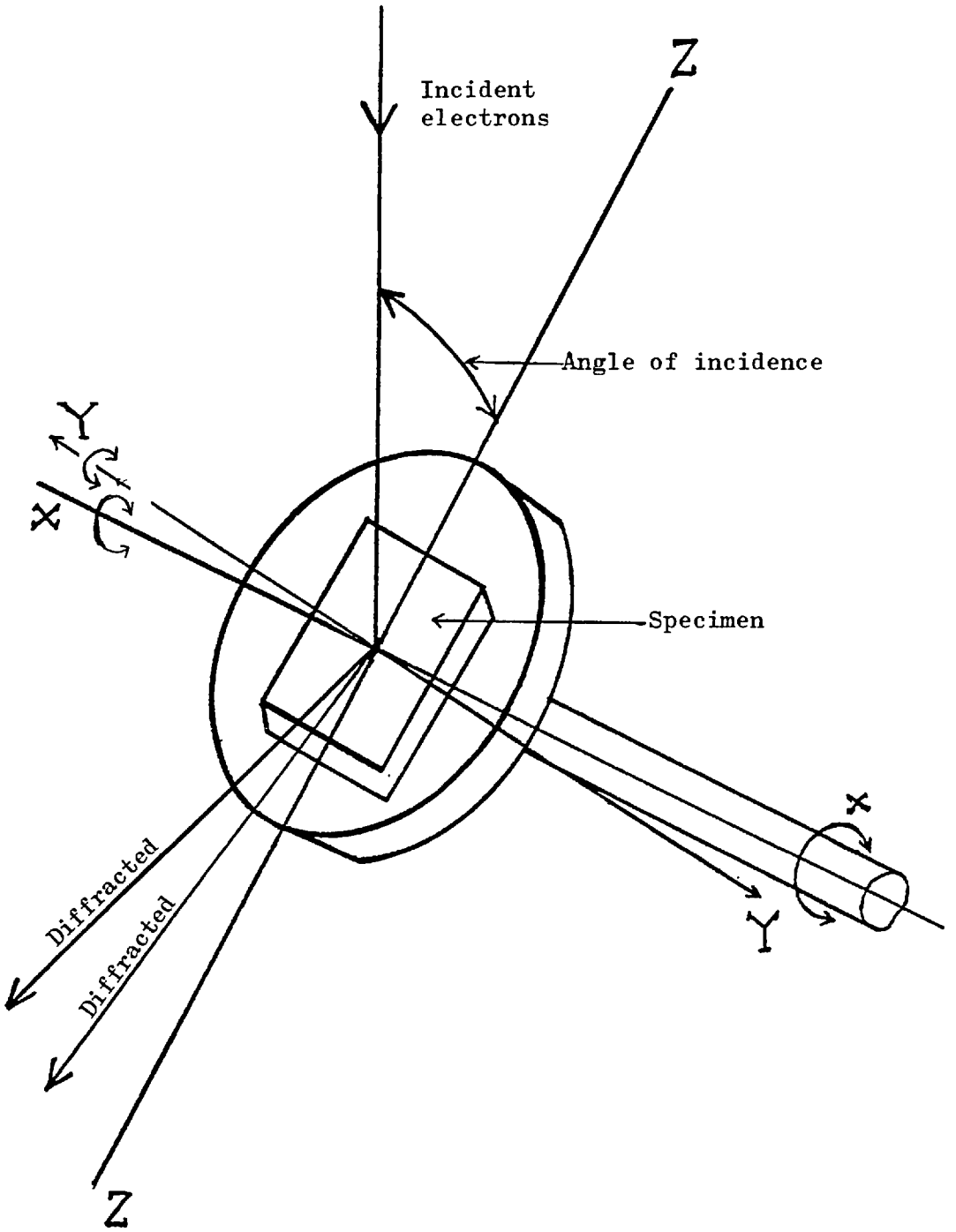


FIG. 3.1 Specimen holder.

Note: The axis XX is perpendicular to the plane containing the surface of the specimen; YY lies in this plane. The line ZZ also lies in the surface plane and is at right angles to XX and YY.

CHAPTER 4

EXPERIMENTAL PROCEDURE

4.1 PREPARATION OF SPECIMENS - GENERAL

The method for measuring the inner potential used here requires an electron beam to make a small glancing angle with the surface of the specimen. To be effective, the surface of the specimen must be sufficiently flat, on an atomic scale to ensure that the electron beam will enter and leave the same flat region of the surface (see Fig. 4.1a). Spurious values may result if the surface is not flat, the electrons entering and leaving the crystal through different faces, as shown in Fig. 4.1b.

4.1.1 Preparation of Copper, Silver and Gold Specimens

These were prepared by deposition onto the surface of freshly cleaved mica or magnesium oxide substrates in a conventional vacuum evaporator at a residual pressure of $\sim 10^{-6}$ torr ($\sim 1.4 \times 10^{-4}$ Pascals). Deposition rates were $\sim 1000 A^{\circ}$/min. For copper, silver and gold the substrate temperatures were approximately $500^{\circ}C$, $250^{\circ}C$ and $450^{\circ}C$ respectively. It was necessary to anneal copper and gold specimens for about twenty hours to ensure a flat surface.

4.1.2 Specimens of Diamond

Only superficial cleaning of the surfaces was required. One diamond had a natural (111) cleavage face which was sufficiently flat, the other two having artificially polished faces.

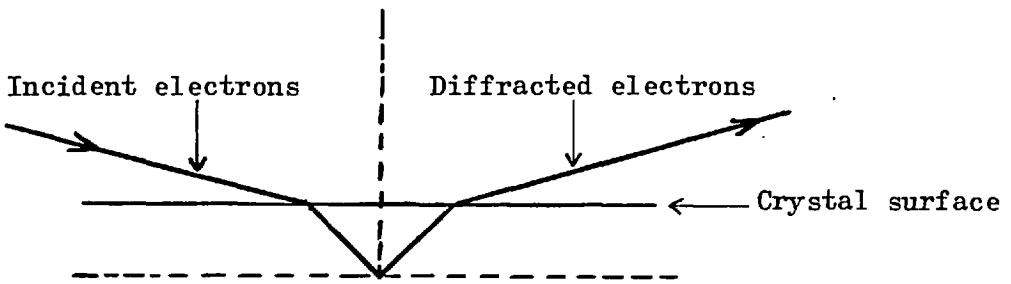


FIG. 4.1a

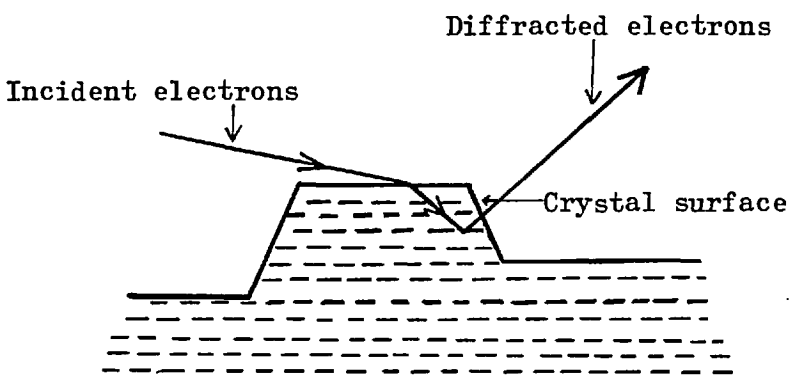


FIG. 4.1b

4.1.3 Specimens of sodium chloride, potassium bromide and calcium fluoride

Good flat surfaces were obtained by cleaving with a knife edge.

4.1.4 Mounting of specimens

Specimens of about one square cm. or less, were fixed to the specimen holder by means of "Aquadag" or "Silverdag". These materials act not only as adhesives but because of their good conducting properties prevent gross charging of those specimens which were bad electrical conductors, e.g. diamond and fluorite.

4.2 PHOTOGRAPHIC RECORDING - GENERAL

An electron beam of about 40 KV energy was directed to make a grazing angle of incidence with the surface of the specimen and diffraction patterns were observed on the fluorescent screen of the camera. Photographic records were made by removing the fluorescent screen from the path of the electrons so as to allow them to fall onto a photographic plate situated below.(see Chapter 3). Photographic plates were developed in an Ilford PQ Developer.

4.2.1 Recording of Bragg spots

Before exposing a photographic plate, the specimen was set (usually) on an azimuth where relatively few Kikuchi lines etc. appeared. (It is possible that, due to dynamical effects, the presence of Kikuchi features may displace a Bragg diffraction spot from its true position.) To lessen the possibility of the electro-

static charging of the photographic plate, the undeflected electrons were sometimes intercepted by interposing a "beam stopper" consisting of a disc of copper foil, between the electrons and the plate. Electrostatic charging of the photographic plate, if it occurs, would lead to a displacement of the Bragg spots away from their true positions, thus increasing the distance between the diffracted and central spots. This in turn would lead to an error in the measurement of the inner potential giving a result lower than the proper value. During the photographic recording, for the continuous rotation method (see Chapter 2), the specimen was turned smoothly from a lower to a higher angle of incidence. The rate of rotation was reduced as the angle was increased, thus compensating for the reduced spot intensity associated with higher order Bragg spots. The total time of exposure was about 5 seconds. For the "Individual Setting" method (see Chapter 2), exposure times were varied from about a half second to about two seconds according to the strength of the Bragg spot being recorded.

For either method, when the beam stopper had been used to intercept the undiffracted electrons (during the photographic recording of the Bragg spots), the position of the central spot was recorded separately. This was done by removing the beam stopper after the crystal had been rotated to a low angle of incidence and subsequently exposing the plate for two or three seconds.

Typical rotation photographs taken from (111) surfaces of copper and gold are shown in Fig. 4.2 and Fig. 4.3 respectively.

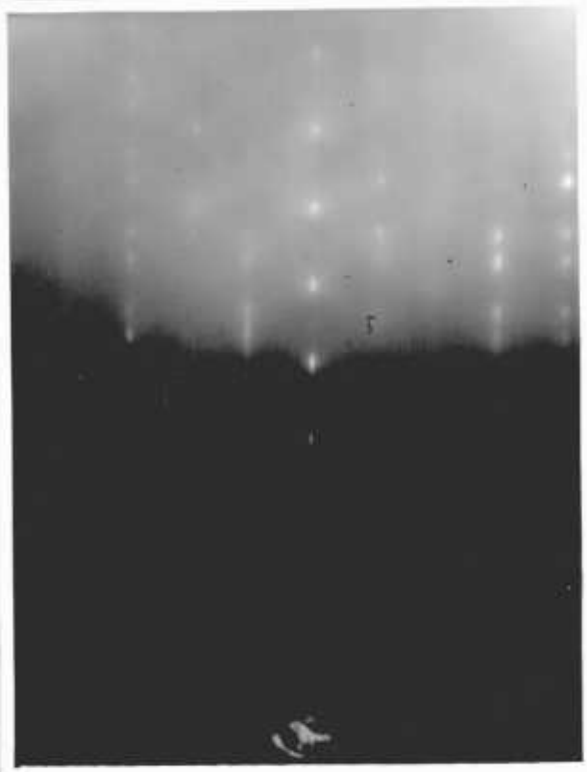


FIG. 4.2

Rotation photograph showing a sequence of Bragg spots from the (111) surface of copper film grown epitaxially on mica.

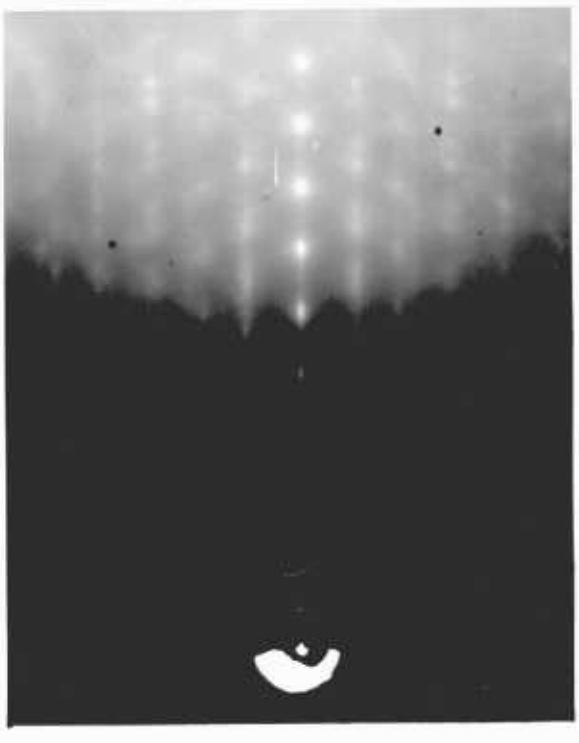


FIG. 4.3

Rotation photograph showing a sequence of Bragg spots from the (111) surface of a gold film grown epitaxially on mica.

4.2.2 Recording of horizontal Kikuchi lines

As for the Yamaguti method, an azimuthal position of the crystal was chosen so that relatively few Kikuchi features (other than horizontal lines) were present. The angle of incidence was then set so as to bring one of the lines into coincidence with its corresponding Bragg diffraction spot. (The reason for doing this is given in Chapter 2, Section 2.3.) The lines were then photographed. The process was repeated with other settings of the angle of incidence using different Bragg spots.

4.3 MEASUREMENTS - GENERAL

After processing the plates, positions of the central spots on the photographic plates were rendered visible by local photographic reduction. After this treatment, the central spot appeared as a small transparent hole in the emulsion so that measurements based on distances of diffracted spots from the central spot could be made easily using a travelling microscope. These distances (r_m^* and r_n^*) for the different order Bragg spots and horizontal Kikuchi lines along the central line were measured several times and the average taken. For measuring purposes, each photographic plate was clamped under the travelling microscope in such a way that the tip of the setting line seen through the eyepiece moves along the central line (Fig. 4.4a and Fig. 4.4b).

The camera length, i.e. the distance between the specimen and the photographic plate, was also measured as accurately as possible.

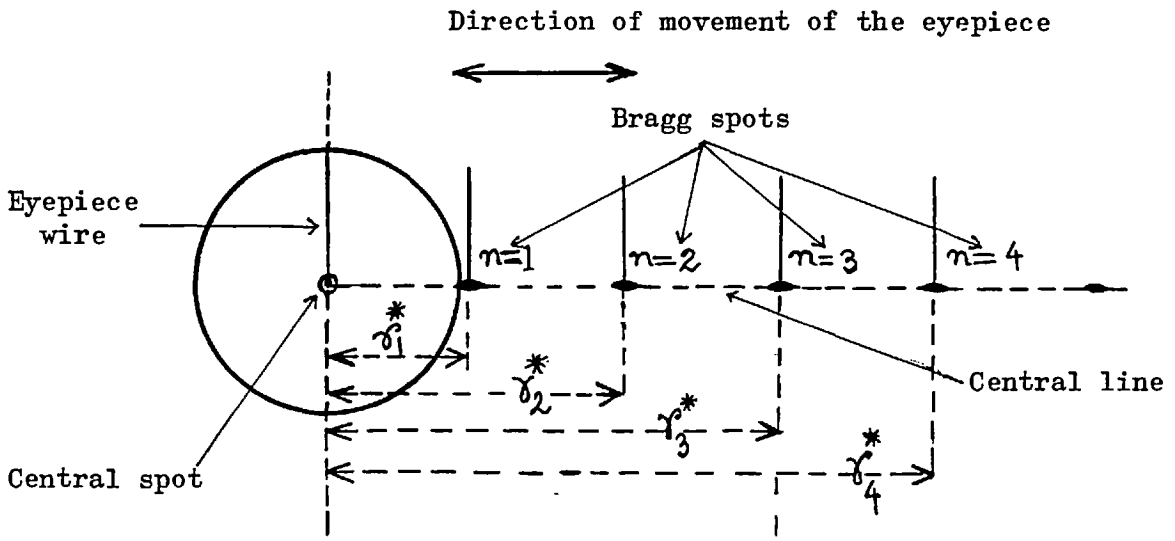


FIG. 4.4a

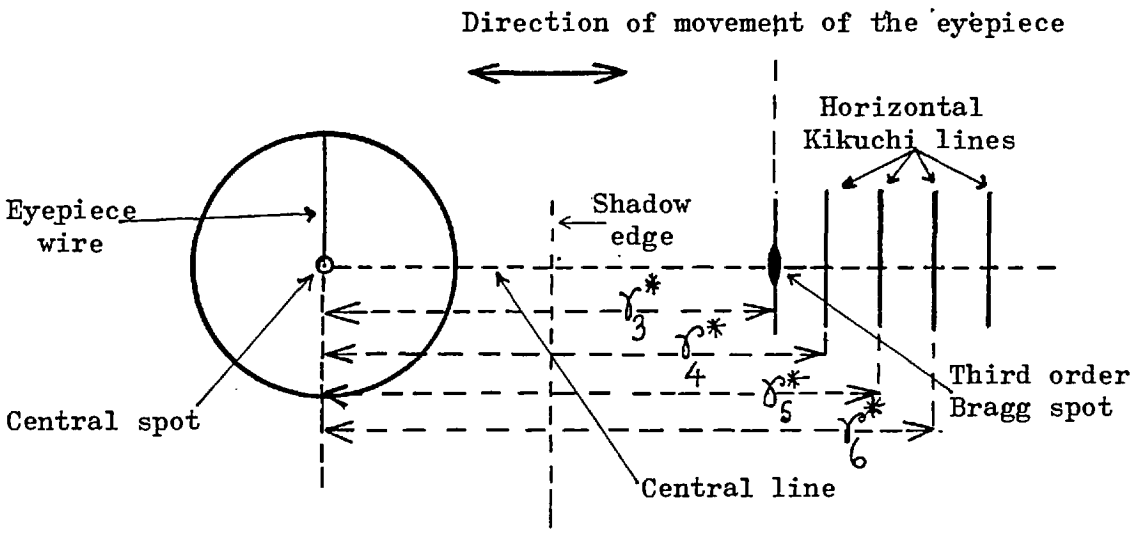


FIG. 4.4b

4.3.1 Treatment of the readings

From the r_n^*'s, the values of $\sin^2\beta_n$ for different orders were calculated using equations (2.5) and (2.8) of Chapter 2. The accelerating potential as indicated by a voltmeter on the E.H.T. supply was used to obtain the approximate value of wavelength λ_o' (Pinsker 1953). The value of each different order using d_{hkl} (Wyckoff 1960) and hence each $(\mu_n^2 - 1)$ was found using equation (2.6) of Chapter 2. The quantities $(\mu_n^2 - 1)$ were plotted against n^2 (see Chapter 2, Section 2.2) usually for $n \geqslant 4$, orders up to the third being ignored as these are usually less distinct. For this reason, their associated distances cannot be measured with sufficient accuracy to give reliable $(\mu_n^2 - 1)$ values. The 'best straight line' through these points is obtained in all cases by the method of "least mean squares" as follows.

Suppose there are points having ordinates $Y_1, Y_2, Y_3, \ldots, Y_n$ corresponding to abscissae $X_1, X_2, X_3, \ldots, X_n$. The best straight line has, say, an intercept a_o with the Y axis and a slope a_1. The values of a_o and a_1 can be evaluated by solving the following equations:

$$\begin{aligned} \Sigma Y - a_o n - a_1 \Sigma X &= 0 \\ \Sigma YX - a_o \Sigma X - a_1 \Sigma X^2 &= 0 \end{aligned} \qquad (4.1)$$

The intercept a_o gives (μ^2-1) and from the slope a_1 the correct wavelength λ_o can be found. Using (μ^2-1) and λ_o so obtained, the value of $\bar{\Phi}$ is calculated by using equation (2.8) of Chapter 2).

4.3.2a Typical calculation for a Yamaguti type experiment on gold

The specimen consisted of a layer of gold, (111) face, deposited on mica.

Lattice spacing $a_o = 4.07825A^o$ (25^oC)

$$d_{111} = \frac{a_o}{\sqrt{3}} = 2.355A^o.$$

Approximate accelerating potential, $P = 45 \times 10^3$ volts.

Approximate wavelength, $\lambda_o' = .057A^o$.

Theoretical considerations indicate that $\bar{\Phi}$ value for gold is probably between 20 and 25 volts (see Chapter 6). Using a value of 20 volts shows that the first order diffraction is suppressed and Bragg spot first shown is in fact the second (222) order. (Generally orders from n = 2 to n = 10 were observed on the photographic plates.) Camera length L = 25.23 cm.

The different values of μ_n^2-1 from Table 4.1 are plotted against the corresponding values of n^2 (see Fig. 4.5) and the best straight line obtained as explained in Fig. 4.3.1. Taking $n^2 = X$ and $(\mu_n^2-1) \times 10^5 = Y$, then from the data of Table 5.1:

$$\begin{aligned} \sum X &= \sum n^2 = 371 \\ \sum X^2 &= \sum (n^2)^2 = 25235 \\ \sum Y &= \sum (\mu_n^2-1) \times 10^5 = 382.74 \\ \sum YX &= \sum n^2(\mu_n^2-1) \times 10^5 = 20276.03 \end{aligned} \qquad (4.2)$$

Substituting the data from equation (4.2) into equation (4.1) gives $a_1 = -1.649318 \times 10^{-3} = (\lambda_o'^2 - \lambda_o^2)/4d^2$, leading to

n = Order of Diffraction	$n^2 = X$	X^2	r_n (cm.)	θ_n (degrees)	$\sin^2\theta \times 10^5$	$n^2 \lambda_5'^2/4d^2$	$(\mu_{n_5}^2 - 1) \times 10^5 = Y$	YX
4	16	256	2.150	2.435	180.49	234.41	53.92	862.72
5	25	625	2.835	3.205	312.66	366.27	53.61	1340.25
6	36	1296	3.491	3.939	471.82	527.43	55.61	2001.96
7	49	2401	4.143	4.663	661.03	717.89	56.86	2786.14
8	64	4096	4.806	5.392	883.11	937.66	54.55	3491.20
9	81	6561	5.464	6.110	1132.76	1186.72	53.96	4370.76
10	100	10000	6.124	6.822	1410.86	1465.09	54.23	5423.00

TABLE 4.1

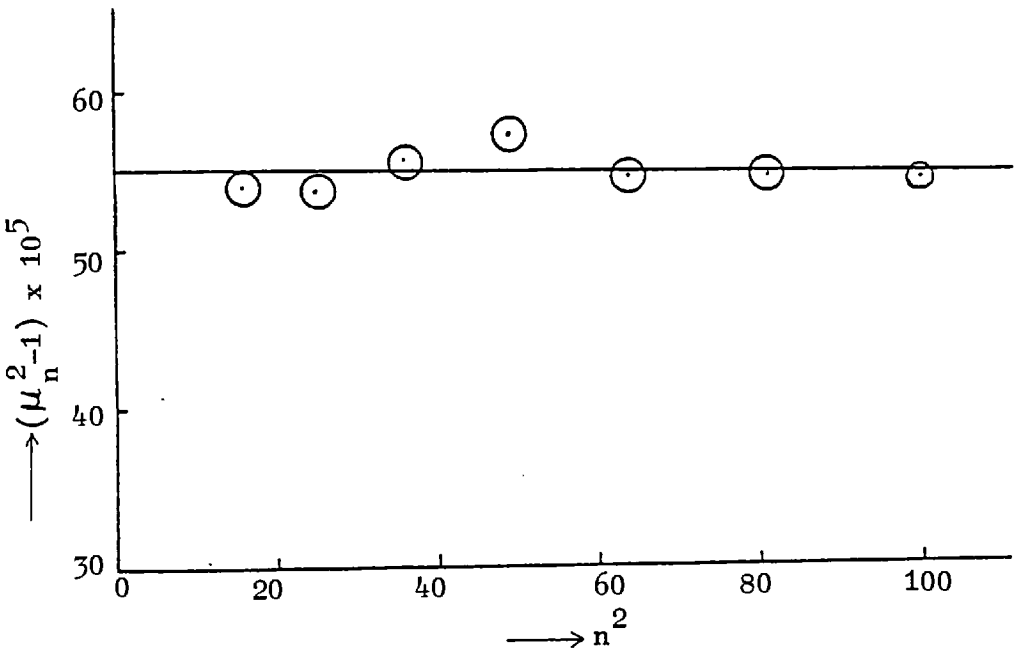

60
50
40
30
0
20
40
60
80
100
$\longrightarrow (\mu_n^2-1) \times 10^5$
$\longrightarrow n^2$

FIG. 4.5

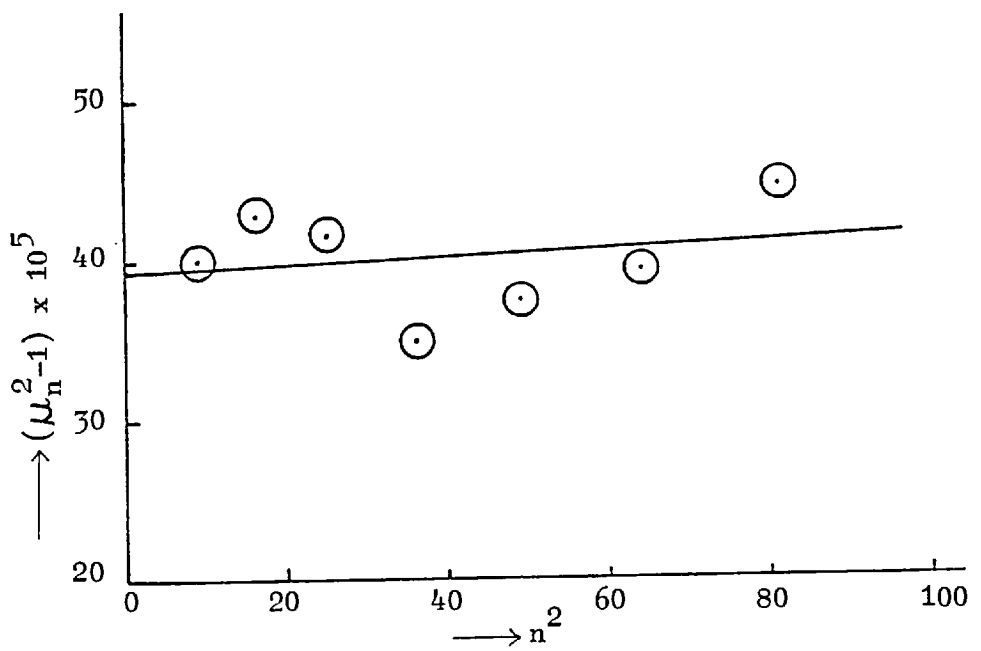

50
40
30
20
0
20
40
60
80
100
$\longrightarrow (\mu_n^2-1) \times 10^5$
$\longrightarrow n^2$

FIG. 4.6

$\lambda_o = .05700^oA$, and $a_o = 54.7646 = (\mu^2-1) \times 10^5$. Using equation (2.8) of Chapter 2:

$$\Phi = \frac{(54.7646 \times 10^{-5}) \times h^2}{2em_o \times 32.4937 \times 10^{-24}} \times \left[1 + \frac{h^2}{m_o^2c^2 \times 32.4937 \times 10^{-24}}\right]^{-\frac{1}{2}}$$

$$= 23.3 \text{ volts.}$$

4.3.2b Typical calculation for a Shinohara type experiment on diamond

Specimen - diamond (111 natural face).

Lattice spacing $a_o = 3.56679A^o$.

Approximate accelerating potential = 40 kV.

Approximate wavelength $\lambda_o' = .0595A^o$.

From Table 4.2 the $(\mu_n^2-1) \times 10^5$ values are plotted against the corresponding n^2 values. The best straight line based on the least mean square procedure is shown in Fig. 4.6. From the intercept and slope the following values are obtained:

$$\mu^2-1 = 39.35 \times 10^{-5}$$

and $$\lambda_o = .05948A^o$$

and making use of equation (2.8) of Chapter 2, we get:

$$\Phi = 15.5 \text{ volts.}$$

Order number n	n^2 =X	r_m^* (cm)	$\frac{1}{2}\tan^{-1}\frac{r_m^*}{L}$ (deg.)	$\tan^{-1}\frac{r_n^*}{L}$ (deg.)	β_n (deg.)	$\sin^2\beta_n \times 10^5$	$\frac{n^2\lambda'^2}{4d^2 \times 10^5}$	$(\mu_n^2 - 1) \times 10^5$
3	9	3.843		8.741	2.203	147.76	187.84	40.08
4	16	4.241		9.630	3.092	290.95	333.93	42.98
5	25	4.639		10.512	3.974	480.30	521.77	41.47
6	36	5.038		11.394	4.856	716.59	751.35	34.76
7	49	5.421		12.235	5.697	985.41	1022.67	37.26
8*	64	5.807	6.538	13.076	6.538	1296.46	1335.74	39.28
9	81	5.790		13.909	7.371	1645.93	1690.54	44.61

* indicates the line coinciding with the corresponding Bragg spots.

TABLE 4.2

CHAPTER 5

EXPERIMENTAL RESULTS

5.1 GENERAL

Measurements of the inner potential have been carried out on the following substances:

i) Copper, silver, gold and diamond.

ii) Potassium bromide, sodium chloride, calcium fluoride and silicon - see Sections 5.9 and 5.10.

5.2 NOTE ON CAMERA LENGTH

The accurately determined distance between the sensitized surface of the photographic plates and the azimuthal axis of the specimen holder, i.e. the 'camera length' was found to be 25.23 cm., but there is always some doubt about the precise camera length for any one experimental result because of the size of the specimen and the type of experiment (see Fig. 5.1). For this reason a nominal value of 25 cm. has been used in the following calculations, but as is shown in Appendix 2, Part B, errors of $\pm$ 5 mm. do not materially alter the results.

5.3 NOTE ON ELECTRON BEAM ENERGY

The accelerating potentials used were usually between 40 and 50 kV, although 20 kV was used on some of the measurements on silver to check for the possibility of the inner potential changing with the beam energy. Within the errors of measurement no difference was obtained in the range 20 to 50 kV (see Tables 5.2, 5.3 and 5.4).

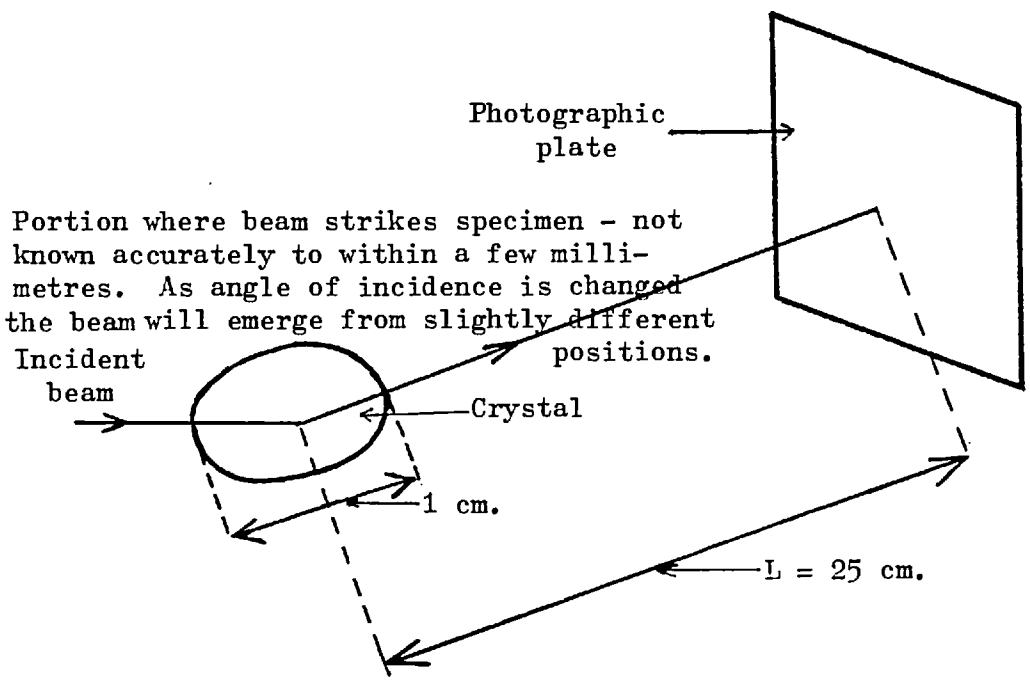

Photographic plate
Portion where beam strikes specimen - not known accurately to within a few millimetres. As angle of incidence is changed the beam will emerge from slightly different positions.
Incident beam
Crystal
1 cm.
L = 25 cm.

FIG. 5.1

5.4 PRESENTATION OF THE RESULTS

The results (see typical detailed calculation in Chapter 4, Sections 4.3.1 and 4.3.2) for each substance are summarized in the tables and shown in the form of a histogram.

For the category (I) substances, the results are summarized in Section 5.9.

5.5 COPPER

TABLE 5.1

Cu (111) face (on mica) - Yamaguti method

Approximate accelerating potential - 45 kV.

Specimen no.	$\bar{\Phi}$ in volts for plate no.				
	1	2	3	4	5
1	13.5	13.0	12.2	13.2	14.5
2	14.7	14.0	13.4	13.5	14.7
3	13.0	13.6	-	13.6	12.6
4	12.7	14.0	14.1	12.6	-
5	13.1	12.9	14.2	-	13.6
6	13.1	12.3	15.2	12.9	13.4
7	13.7	14.0	13.9	11.9	-
8	13.3	14.5	13.5	13.0	-
9	12.0	12.4	12.5	-	12.9
10	13.7	13.6	13.9	12.5	13.5
11	13.3	12.1	13.8	12.8	14.0

$\bar{\Phi}$ Average = 13.4 volts $\pm$ 0.8 volts

5.6 SILVER

TABLE 5.2

Silver (111) face (on mica) - Yamaguti method

Approximate accelerating potential - 20 kV

Specimen number	$\bar{\Phi}$ in volts for plate no.				
	1	2	3	4	5
1	17.1	18.3	16.0	16.3	-
2	15.8	16.1	17.8	19.8	-
3	18.1	18.1	19.4	19.3	-
4	17.3	17.8	18.9	19.2	-
5	17.4	17.5	18.4	-	-
6	18.0	18.0	18.4	-	-

$\bar{\Phi}$ Average = 17.9 volts $\pm$ 1.1 volts

TABLE 5.3

Approximate accelerating potential - 40 kV

Specimen number	$\bar{\Phi}$ in volts for plate no.				
	1	2	3	4	5
1	17.5	17.0	17.2	-	-
2	18.5	17.6	17.1	17.3	18.0
3	16.4	18.0	18.0	18.4	-
4	16.8	16.8	17.1	17.5	17.2
5	18.2	18.3	17.6	18.2	17.6
6	18.0	17.6	17.0	-	-
7	18.9	18.0	16.2	17.7	17.7

$\bar{\Phi}$ Average = 17.6 volts $\pm$ 0.6 volts

TABLE 5.4

Approximate accelerating potential = 45 kV

Specimen number	$\bar{\Phi}$ in volts for plate no.				
	1	2	3	4	5
1	17.4	17.0	18.0	19.4	-
2	17.6	18.2	18.2	18.3	-
3	16.4	18.7	18.3	16.3	-
4	16.2	18.3	19.7	17.0	-
5	17.2	15.7	16.5	17.5	-
6	16.6	16.8	16.7	18.1	16.9
7	20.1	18.2	19.7	19.8	-
8	18.3	17.9	19.3	17.3	-
9	17.3	16.3	17.6	18.1	-
10	18.5	18.1	18.3	-	-
11	17.6	18.5	18.2	-	-

$\bar{\Phi}$ Average = 17.8 volts $\pm$ 1.1 volts

TABLE 5.5

Silver (111) face (on MgO) - Yamaguti method

Approximate accelerating potential = 45 kV

Specimen number	$\bar{\Phi}$ in volts for plate no.				
	1	2	3	4	5
1	17.2	16.3	16.3	16.3	16.3
2	16.9	16.8	17.7	-	-
3	17.9	16.9	16.9	16.7	16.8
4	16.4	17.0	17.1	16.8	-
5	17.0	18.3	18.6	18.6	-
6	17.6	18.6	17.4	17.8	-

$\bar{\Phi}$ Average = 17.2 volts $\pm$ 0.8 volts

Measurements on silver using accelerating potentials from 20 kV to 45 kV gave similar results within the limits of experimental error.

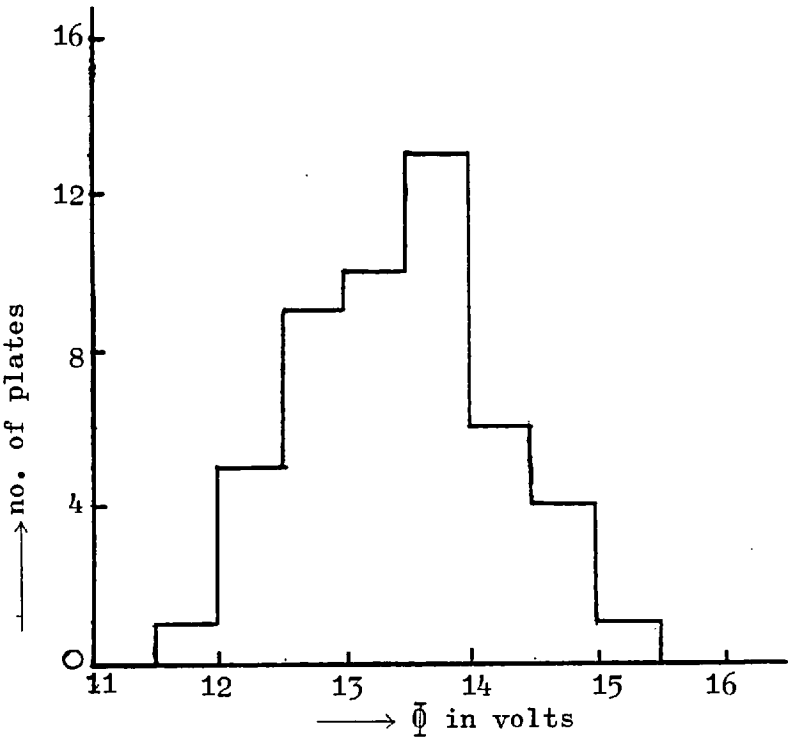


FIG. 5.2 Histogram for copper (from Table 5.1).

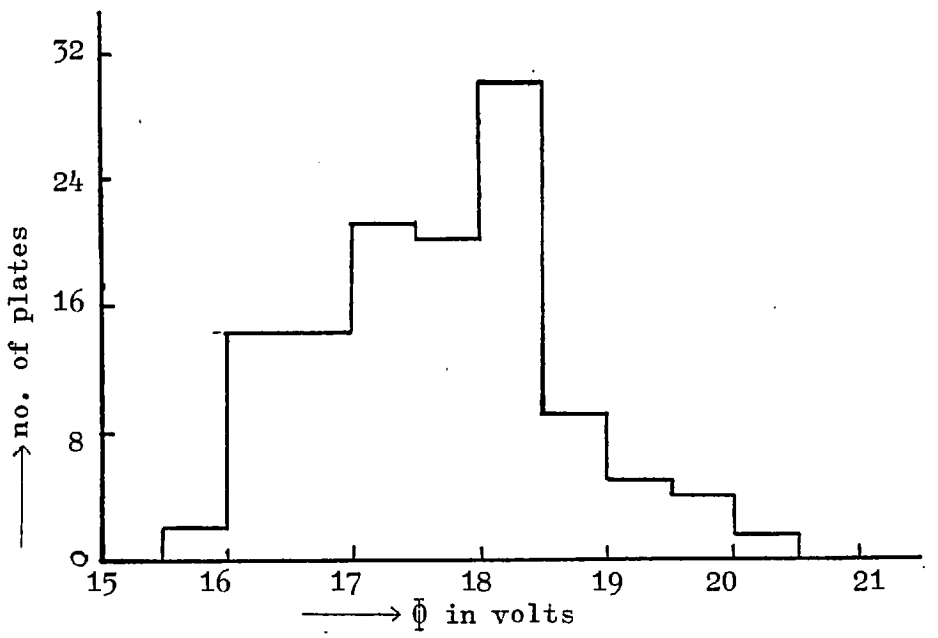


FIG. 5.3 Histogram for silver (from Tables 5.2, 5.3, 5.4 and 5.5).

5.7 GOLD

TABLE 5.6

Gold (111) face (on mica) - Yamaguti method

Approximate accelerating potential = 45 kV

Specimen number	$\bar{\Phi}$ in volts for plate no.				
	1	2	3	4	5
1	21.6	21.3	21.2	20.5	21.3
2	20.5	21.2	21.8	23.4	-
3	21.3	23.4	22.7	21.2	21.1
4	21.9	22.8	22.4	20.2	-
5	22.2	21.5	22.2	21.9	22.4
6	22.4	21.6	21.9	21.4	23.4
7	21.1	20.6	21.0	21.8	-
8	20.1	19.6	-	-	-
9	21.8	21.5	21.5	21.6	-
10	22.1	21.8	22.4	21.0	-
11	22.0	22.4	22.6	24.3	-

$\bar{\Phi}$ Average = 21.7 volts $\pm$ 0.9 volts

TABLE 5.7

Gold (111) face (on MgO) - Yamaguti method

Approximate accelerating potential = 45 kV

Specimen number	$\bar{\Phi}$ in volts for plate no.				
	1	2	3	4	5
1	19.5	19.3	19.1	20.4	-
2	22.0	21.3	21.2	21.8	22.6
3	22.0	22.1	21.5	21.4	-
4	21.6	21.4	21.1	21.9	-
5	19.4	21.2	18.2	21.3	-
6	18.5	20.0	20.0	21.2	-
7	22.8	22.4	22.3	19.7	-
8	22.3	20.2	22.1	20.8	-

$\bar{\Phi}$ Average = 21.0 volts $\pm$ 1.2 volts

5.8 DIAMOND

TABLE 5.8

Diamond (100) face

Yamaguti method (rotation and individual setting)

Approximate accelerating potential = 45 kV

Plate no.	$\bar{\Phi}$ in volts	Plate no.	$\bar{\Phi}$ in volts
1	16.4	24	14.9
2	13.3	25	14.8
3	14.2	26	17.6
4	12.1	27	15.5
5	16.3	28	14.7
6	14.3	29	13.6
7	12.1	30	14.9
8	12.9	31	13.5
9	12.8	32	17.8
10	15.0	33	15.9
11	14.0	34	17.8
12	14.7	35	15.6
13	12.2	36	16.0
14	16.0	37	15.0
15	12.7	38	17.3
16	12.0	39	14.9
17	12.6	40	17.2
18	13.4	41	12.3
19	12.5	42	14.1
20	12.8	43	16.2
21	15.4	44	13.7
22	14.7	45	11.8
23	15.6	-	-

$\bar{\Phi}$ Average = 14.5 volts $\pm$ 1.7 volts

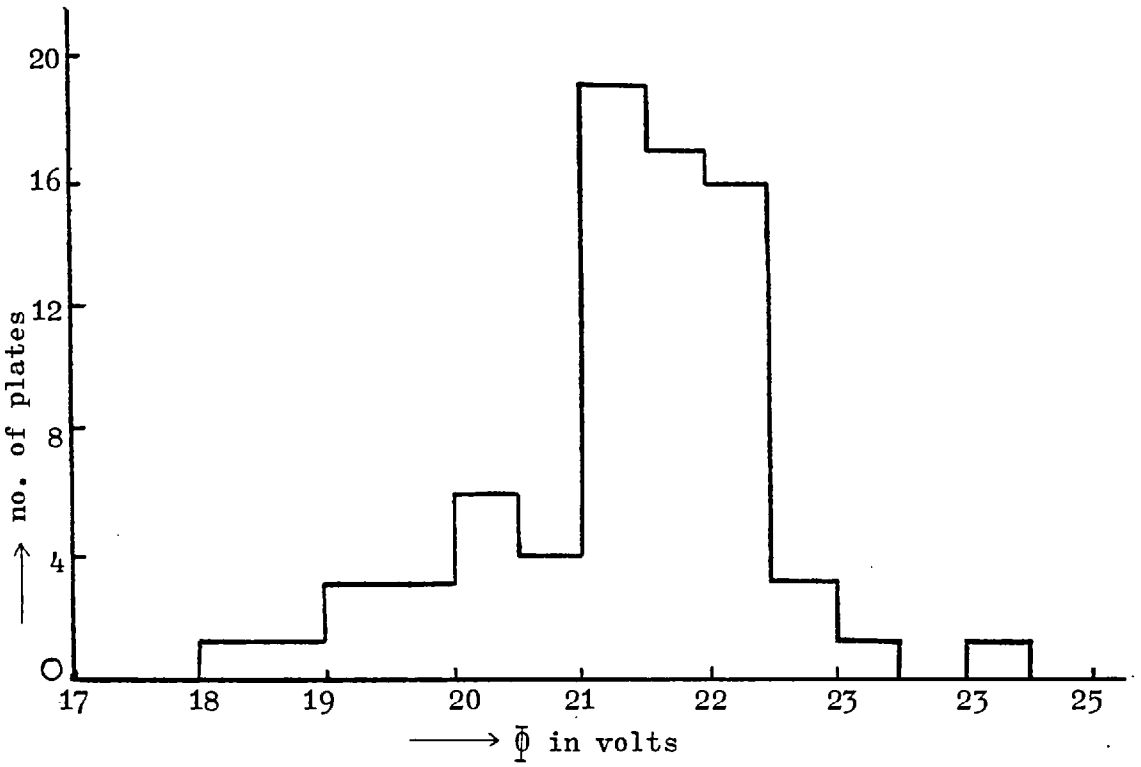


FIG. 5.4 Histogram of gold (from Tables 5.6 and 5.7).

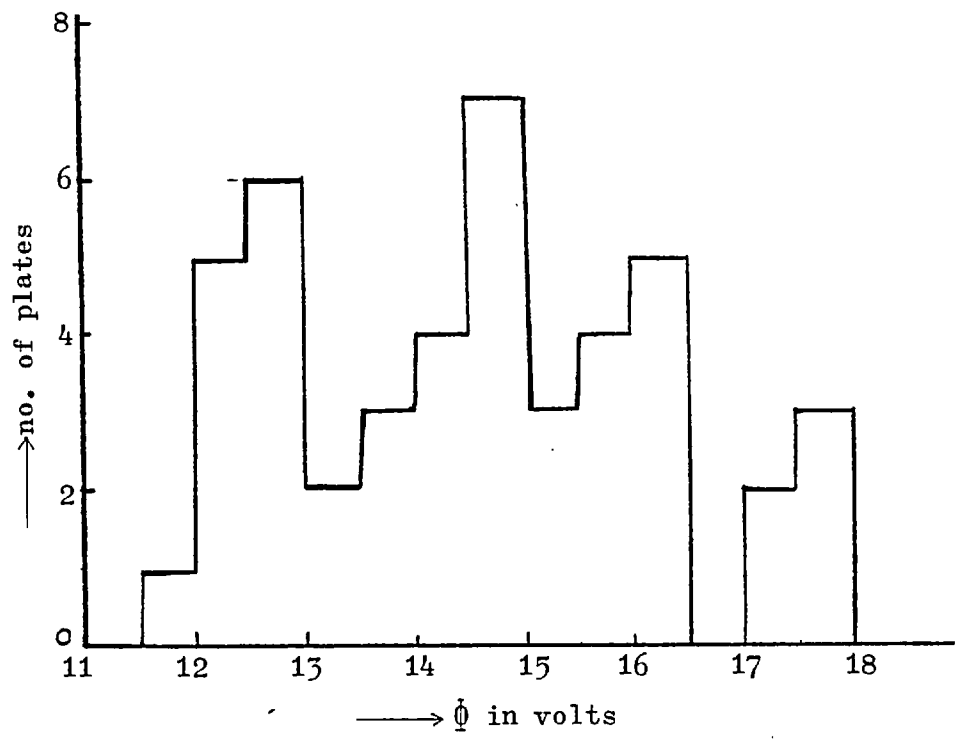


FIG. 5.5 Histogram for diamond (100) face (from Table 5.8).

TABLE 5.9

Diamond (111) face - Yamaguti method

Approximate accelerating potential = 45 kV

(Rotation up to plate no. 45 and individual setting up to plate no. 66)

Plate no.	$\bar{\Phi}$ in volts	Plate no.	$\bar{\Phi}$ in volts
1	14.3	34	14.3
2	16.5	35	13.4
3	14.2	36	13.6
4	15.7	37	14.4
5	13.3	38	15.0
6	13.5	39	10.7
7	17.7	40	13.6
8	16.7	41	10.7
9	12.4	42	15.3
10	15.7	43	15.6
11	15.0	44	12.8
12	14.2	45	14.8
13	15.5	46	18.1
14	15.9	47	18.4
15	14.6	48	16.0
16	13.9	49	17.9
17	15.7	50	16.5
18	15.8	51	15.0
19	14.6	52	17.8
20	14.9	53	16.5
21	15.7	54	15.0
22	15.3	55	19.5
23	14.3	56	14.5
24	12.9	57	16.5
25	13.7	58	15.5
26	15.4	59	15.5
27	15.3	60	19.4
28	13.1	61	15.8
29	15.2	62	17.2
30	12.3	63	16.3
31	12.5	64	17.9
32	14.5	65	16.5
33	17.7	66	18.2

$\bar{\Phi}$ Average = 15.2 ± 1.9 volts

TABLE 5.10

Diamond (111) face

Shinohara's method

Approximate accelerating potential = 40 kV

Φ in volts for plate no.				
1	2	3	4	5
17.6	13.8	15.5	17.3	16.2
12.7	15.6	17.6	18.4	16.7
18.3	18.9	18.2	17.2	14.6
18.0	18.0	15.4	18.8	18.0
19.1	19.2	17.8	17.8	18.1
18.0	15.9	16.2	18.3	16.7
16.5	18.4	17.4	18.6	15.5
18.5	17.7	18.5	16.5	16.7
20.2	18.2	18.6	16.6	17.0

Φ Average = 17.3 ± 1.5 volts

TABLE 5.11

Diamond (conducting type) (111) face

Approximate accelerating potential = 40 kV

Experimental method	Φ in volts for plate no.				
	1	2	3	4	5
Yamaguti (rotation)	13.6	15.3	14.8	14.6	-
Yamaguti (rotation)	14.5	16.1	15.1	16.0	-
Yamaguti (individual setting)	14.5	14.5	15.9	14.0	14.6
Yamaguti (individual setting)	14.1	17.5	11.3	11.4	-
Shinohara's method	13.9	14.1	13.8	-	-
Shinohara's method	13.9	14.1	15.4	12.2	14.1
Shinohara's method	12.9	15.0	15.1	11.4	-
Shinohara's method	13.4	11.8	9.5	11.4	12.9

Φ Average = 13.9 ± 1.7 volts

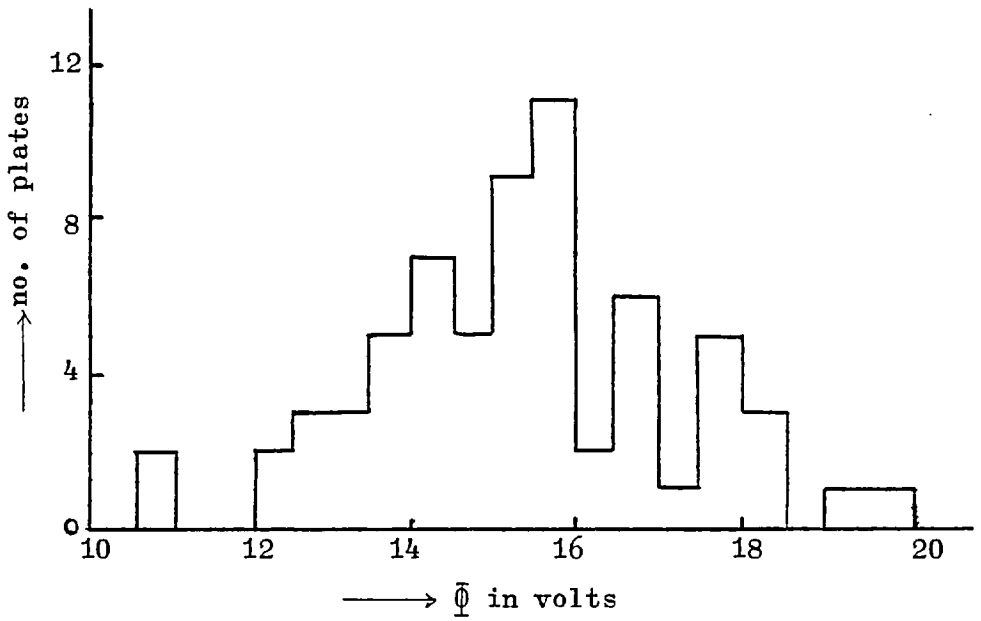


FIG. 5.6 Histogram for diamond (111) face, using Yamaguti method (see Table 5.9).

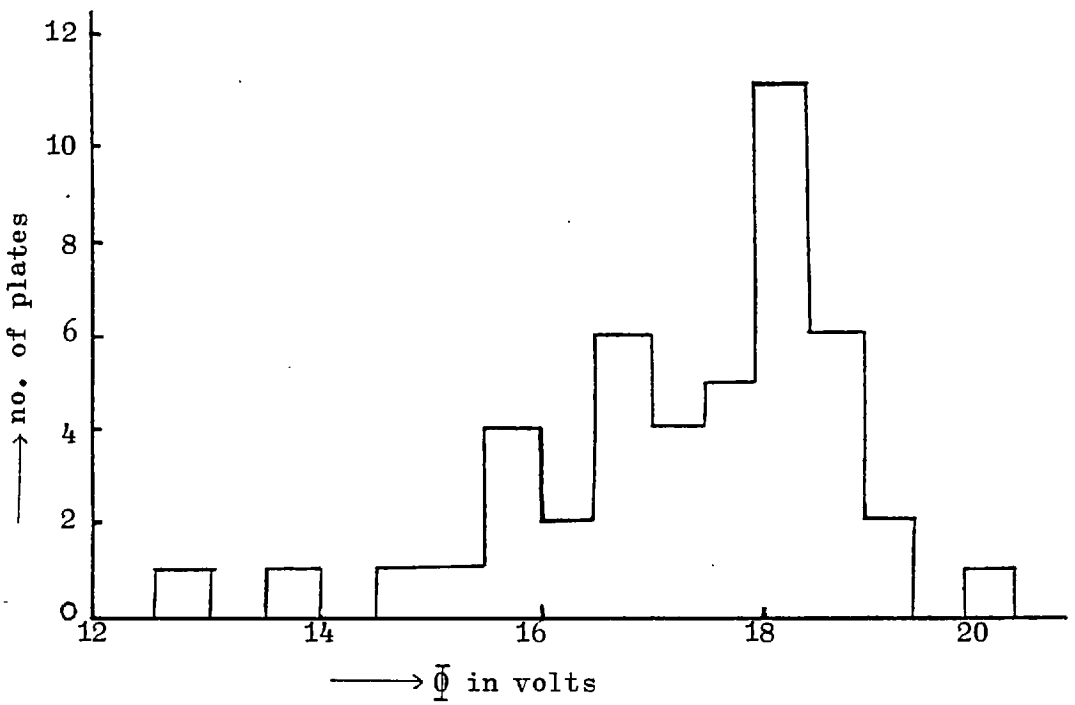


FIG. 5.7 Histogram for diamond (111) face, using Shinohara's method (see Table 5.10).

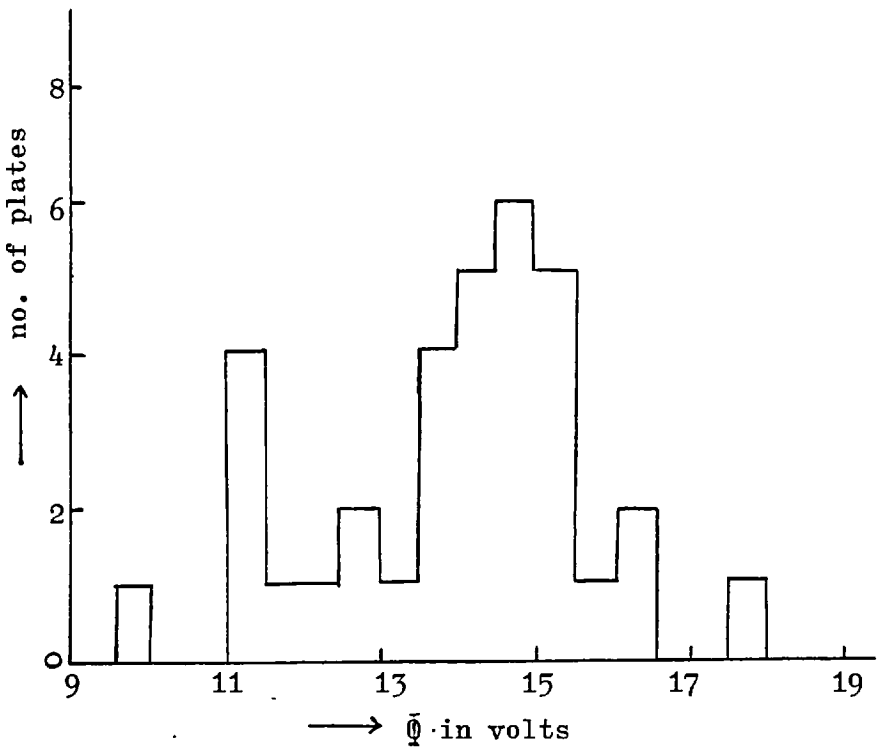


FIG. 5.8 Histogram for diamond (conducting type) (see Table 5.11).

5.9 SUMMARY OF RESULTS FOR COPPER, SILVER, GOLD AND DIAMOND

The measurements of the present work on copper, silver, gold and diamond are summarized in Table 5.12 below.

TABLE 5.12

Specimen	Method used	Number of measurements	Range of values of inner potential (volts)	Average value of inner potential (volts)
1) Cu(111) - on mica	Yamaguti	49	11.9-14.7	13.4 ± 0.8
2) Ag(111) - on MgO	Yamaguti	25	16.3-18.6	17.2 ± 0.8 } 17.7 ± 0.9
3) Ag(111) - on mica	Yamaguti	95	16.2-20.1	17.8 ± 1.0 }
4) Au(111) - on MgO	Yamaguti	33	18.5-22.6	21.0 ± 1.2 } 21.4 ± 1.1
5) Au(111) - on Mica	Yamaguti	46	19.6-24.3	21.7 ± 0.9 }
6) Diamond (000)	Yamaguti	45	11.8-17.8	14.5 ± 1.7
7) Diamond (111)	Yamaguti	66	10.7-19.5	15.2 ± 1.9
8) Diamond (111)	Shinohara	45	12.7-20.2	17.3 ± 1.5
9) Diamond (111) Conducting type	Yamaguti	34	11.3-16.1	13.9 ± 1.7

The difference between the results for the ordinary and the "conducting" diamond is not significant, indicating that the value found for the ordinary diamond has not been affected appreciably by charging.

Because of the appreciable differences between the experimental values obtained from the present work and those from work carried out in the past (see Chapter 1, Table 1.2), the inner potentials of a number of additional substances were carried out as a check. These are presented in Section 5.10.

5.10 RESULTS FOR SODIUM CHLORIDE, POTASSIUM BROMIDE, CALCIUM FLUORIDE AND SILICON

In addition to measuring the inner potentials of silver and gold, Tull (1951a)also measured sodium chloride. Again, Bühner and Sleeb (1967a)measured both sodium chloride and potassium bromide, as well as copper. Kehoe (1957) measured the inner potentials of a series of alkali halides including the two mentioned above. For this reason these two substances have also been investigated. Measurements have also been conducted on silicon and calcium fluoride. The values for the above substances together with those obtained by other workers in the past are given in Table 5.13.

TABLE 5.13

Measurements by	$\bar{\Phi}$ in volts for				Method used
	NaCl	KBr	CaF_2	Si	
1) Tillman (1934)	-	-	11.6	-	Yamaguti's method
2) Tull (1951a)	8.5	-	-	-	Yamaguti's method
3) Kehoe (1957)	6.9	7.3	-	-	Yamaguti's method
4) Buhner and Sleeb(1967a)	8.24	9.05	-	-	Reflection method (Yamaguti)
5) Gaukler and Schwarzer (1971)	-	-	-	11.5	Shinohara's method
6) Menadue (1972)	-	-	-	12.0 ± 0.4	Yamaguti method in U.H.V.
7) Present work	6.4 ± 0.5	7.1 ± 0.5	-	11.8 ± 1.5	Yamaguti's method
8) Present work	-	-	11.8 ± 1.0	-	Shinohara's method

CHAPTER 6

THE THEORETICAL CALCULATION OF INNER POTENTIAL

6.1 GENERAL

The inner potential, the volume average of electrostatic potential inside a crystal, can in principle, be found if the charge distribution inside the crystal is known in detail. However, even if the charge distribution is known to the required degree of accuracy, the work involved would be very great. For this reason, Bethe (1928b) assumed a simplified crystal model composed of free atoms or ions having spherical symmetry for which the inner potential, $\bar{\Phi}$, is given by the formula:

$$\bar{\Phi} = \frac{2\pi e}{3} \sum_i N_i \int_0^\infty \rho_i(r) r^4 dr \qquad (6.1)$$

where e is the electron charge in e.s.u., N_i is the number of atoms or ions of the i^{th} kind per unit volume, $\rho_i(r)$ is the electron density of the i^{th} kind of atom or ion at a distance r from the nucleus. $\rho_i(r)$ is defined in such a way that $\rho_i(r)r^2dr$ is the number of electrons contained in a spherical shell of radius r and thickness dr, so that:

$$\int_0^\infty \rho_i(r) r^2 dr,$$

is the total number of electrons for the atom or ion.

Calculations were carried out on sodium chloride, for example, to evaluate the term under the integral sign in equation (6.1)

with the help of data published by Bearden (1927). These were based on X-ray measurements and gave values of $U_i(r)$, where:

$$U_i(r)dr = \varrho_i(r)r^2dr \qquad (6.2)$$

for various values of r, for the Na^+ and Cl^- ions. Not only did Bearden give two curves for the Cl^- ions, but also all the curves showed small fluctuations about the zero line for larger values of the distance r from the nucleus (see Fig. 6.1). Since $U_i(r)$ must be multiplied by the square of the distance r from the centre of the nucleus to give the term under the integral sign in equation (6.1), these fluctuations can have a very large influence on the resulting value of the inner potential. A series of values ranging from 5.35 volts to 13.55 volts can be obtained for sodium chloride according to which of the Bearden curves is used. No further work has been carried out using these curves.

6.2 THE METHOD OF SHINOHARA AND MIYAKE

Shinohara (1932b) and Miyake used a modification of equation (6.1) by expressing $\varrho_i(r)$ as a Fourier series in terms of atomic scattering factors, and integrating term by term, giving:

$$\bar{\phi} = \frac{2\pi e}{3} \sum_i N_i d^2 \sum_{n=1}^{\infty} F_i(n)(-1)^{n+1} \left[\frac{1}{2} - \frac{3}{\pi^2 n^2} \right] \qquad (6.3)$$

where $F_i(n)$ is the atomic scattering factor for the i^{th} kind of atom or ion for the n^{th} order reflection from crystal planes of spacing d. Equation (6.3) was deduced on the assumption that the parameter d obeyed the condition that:

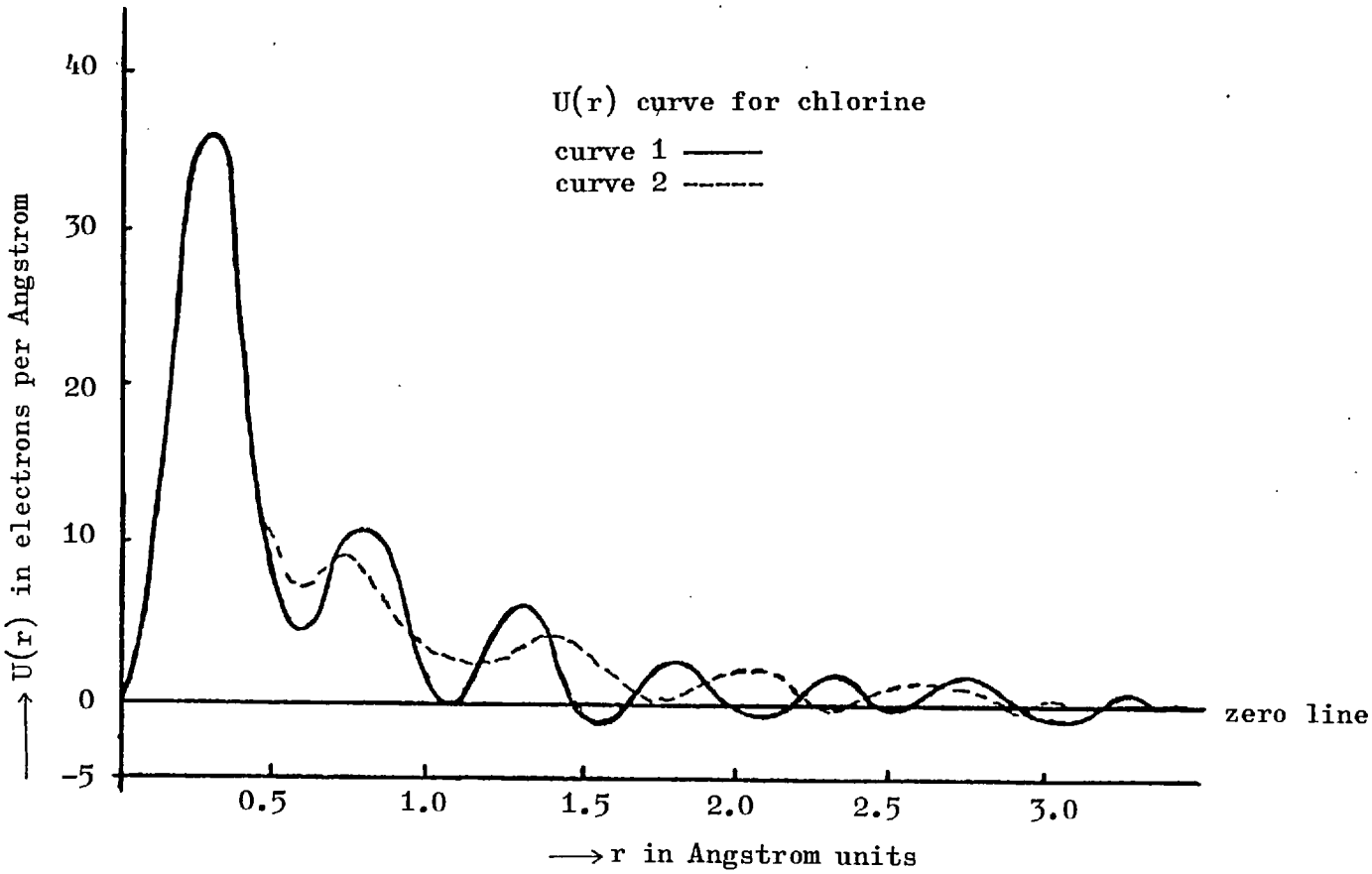

U(r) curve for chlorine
curve 1
curve 2
40
30
20
10
0
-5
0.5
1.0
1.5
2.0
2.5
3.0
zero line
⟶ U(r) in electrons per Angstrom
⟶ r in Angstrom units

FIG. 6.1

$$\rho_i(r) = 0 \quad \text{for} \quad \tfrac{1}{2}d < r \tag{6.4}$$

Since the representation of an algebraic expression by a Fourier series is purely a mathematical process which need have no physical significance, the parameter d need not correspond to a set of planes which really exist inside the crystal; it may be of any value greater than the condition as set by equation (6.4). From equation (6.3) the inner potential of sodium chloride was calculated by using the atomic scattering factors obtained experimentally by Brill, Grimm, Herrmann and Peters (1939) and it was found to vary from 4.4 volts to 10 volts for d ranging from $3A^{o}$ to $7A^{o}$. As experimental values of atomic scattering factors are not accurate enough, and also a small percentage of error in one of the larger terms in the series of equation (6.3) will produce a large percentage error in the final result, it is not possible to get accurate values of the inner potential of a crystal from equation (6.3).

6.3 AN APPROXIMATION FOR THE ATOMIC SCATTERING FACTORS

The difficulties mentioned in Section 6.2 could be overcome if the atomic scattering factors $F_i(n)$ were known to within an accuracy of .01%. Since experimentally obtained values of $F_i(n)$ are not known to such a high degree of accuracy, they cannot be used in equation (6.3) to produce reliable inner potential values.

Tull (1951b) attempted to find a mathematical expression relating the atomic scattering factor $F_i(n)$ and plane spacing d so that the right-hand side of equation (6.3) is independent of d and also to form a satisfactory representation of the data obtained both theoretically and experimentally. According to Tull, a good mathematical expression for this is:

$$F_j(n) = E_j e^{-A_j \frac{\sin^2\theta_n}{\lambda^2}} \qquad (6.5)$$

where $F_j(n)$ and E_j are the atomic scattering factor and number of electrons for the j^{th} electron shell, respectively, and A_j is a constant depending on the type of electron.

When an exponential scattering factor of the type defined by equation (6.5) is used, it is not necessary to evaluate each individual term of a Fourier series for the radial electron density, since the sum can be expressed directly as a function of A_j's, as shown below.

If $\varrho_i(r)$, the electron density function for an electron in the j^{th} shell, can be represented as a Fourier integral as:

$$\varrho_j(r) = \frac{8\pi}{r} \int_0^\infty .F_j(s).\sin(2\pi r.s).s.ds \qquad (6.6)$$

where $s = \frac{1}{d} = 2(\frac{\sin\theta}{\lambda})$,

θ, is the Bragg angle,

and λ, is the wavelength of the electrons,

then if $F_j(s)$ has the form:

$$F_j(s) = e^{-A_j(\frac{\sin^2\theta}{\lambda^2})}$$

(considering a single electron in the shell), then equation (6.6) becomes:

$$\varrho_j(r) = \frac{8\pi}{r} \int_0^\infty e^{-A_j(\frac{\sin^2\theta}{\lambda^2})} .\sin(2\pi rs).s.ds$$

which on evaluation gives:

$$\varphi_j(r) = \frac{(4\pi)^{5/2}}{A_j^{3/2}} e^{-4\pi r^2/A_j} \qquad (6.7)$$

Substituting this equation for $\varphi_j(r)$ in (6.1) gives:

$$\Phi = \frac{2\pi e}{3} \sum_{ij} N_i \int_0^\infty \frac{(4\pi)^{5/2}}{A_j^{3/2}} . e^{-4\pi^2 r^2/A_j} . r^4 dr \qquad (6.8)$$

where the suffix 'j' refers to the electrons in the shell, and the suffix 'i' to the atom or ion, the summation being taken over all the electrons of all atoms or ions in the elementary cell. When evaluated, equation (6.8) becomes:

$$\Phi = \frac{e}{4\pi} \sum_{ij} N_i A_{ij} \qquad (6.9)$$

If there are E_{ij} electrons in the j^{th} electron shell of the i^{th} kind of atom or ion, equation (2.9) becomes:

$$\Phi = \frac{e}{4\pi} \sum_{ij} N_i E_{ij} A_{ij} \qquad (6.10)$$

Thus if the various A_{ij} values are known, equation (6.10) can be used to obtain the inner potential of a given crystal.

This can be done by using the functions given by Pauling (1932), who deduced the atomic scattering factors for any electron of any atom or ion by considering them to have spherical symmetry. Thus to evaluate scattering factors he considered the electron distribution corresponding to the Schrödinger eigen functions for a

hydrogen-like atom. If the scattering factors F_j have the exponential form of equation (6.5) and if $\log(F_j)$ for some particular type of electron is plotted against $\sin^2\theta/\lambda^2$, a straight line should result, the slope of which would give the value of A_{ij}. The A_j values for different shells can be obtained in the same way and hence Φ can be calculated by using equation (6.10).

A sample calculation for the A_j value of 3p shell of Cu is given below.

The expression for $F_j(n)$ for 3p shell of Cu^+ is:

$$F_{3p} = \frac{(1-4x^2)(1-3x^2)(3-x^2)}{3(1+x^2)^6}$$

where: $x = \dfrac{n\pi a_o}{(Z-S_s)D}$,

S_s, is the screening constant for 3p shell of Cu = 12.97,

n, is the total quantum number of the shell concerned,

$D = d/n$.

Z = atomic number

The lattice spacing a_o of Cu = $3.56679A^o$, so that

$$d_{111} = 2.087A^o$$

and $\sin\theta/\lambda = n(1/2d)$

The $\log F_{3p}$ values from Table 6.1 are plotted against the corresponding values of $\sin^2\theta/\lambda^2$ as shown in Fig. 6.2. The best straight line through these points has a slope of 5.417, i.e. A_j for 3p shell = 5.417.

A_j values for the other cells are found in a similar fashion and are given in Table 6.2.

n	D (^{o}A)	$\frac{\sin^2\theta}{\lambda^2_{(A^{o})^{-2}}}.10^2$	x^2	$1 - 4x^2$	$1 - 3x^2$	$3 - x^2$	$\frac{1}{3(1+x^2)^6}$	F_{3p}	$\log F_{3p} \times 10$
1.0	2.087	5.739	.002221	.911161	.933371	2.9778	.292172	.73994	-3.0118
1.1	1.739	8.265	.031988	.872048	.904036	2.96801	.275950	.645687	-4.3744
1.2	1.491	11.25	.0435142	.825943	.869457	2.95649	.258160	.54810	-6.0129
1.3	1.304	14.69	.0568894	.772442	.829332	2.94311	.239167	.450923	-7.96456
1.4	1.16	18.60	.0718903	.712439	.784329	2.92811	.219774	.359592	-10.22785

TABLE 6.1

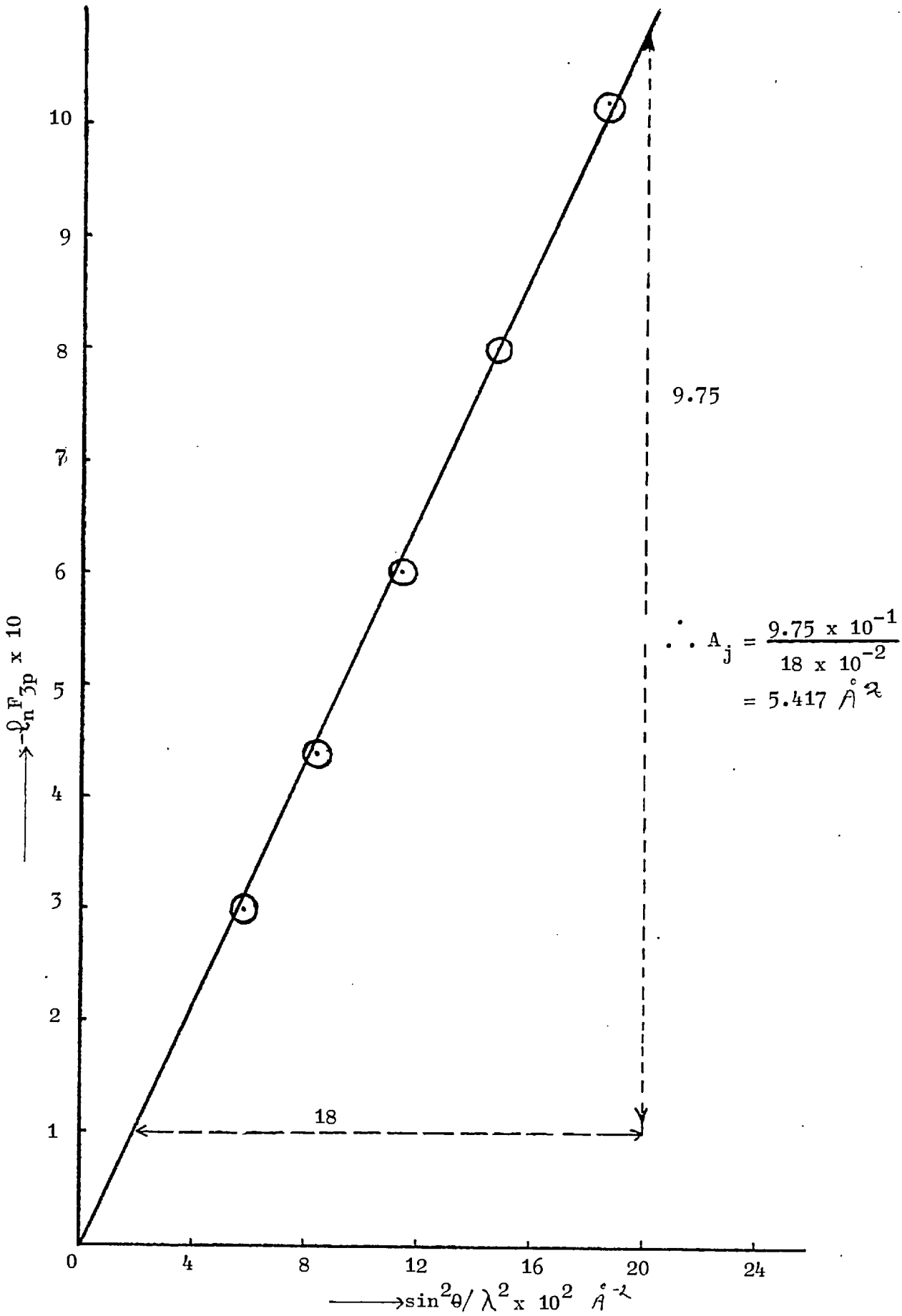

10
9
8
7
6
5
4
3
2
1
0
4
8
12
16
20
24
9.75
18
$\rightarrow -\ell_n F_{3p} \times 10$
$\rightarrow \sin^2\theta/\lambda^2 \times 10^2$ Å^{-2}
$\therefore A_j = \frac{9.75 \times 10^{-1}}{18 \times 10^{-2}}$
$= 5.417$ Å^2

FIG. 6.2

TABLE 6.2

Electron shell	Number of Electrons	A_j (A^{o2} units)	$\bar{\Phi}$ values in volts
1s	2	.026	0.005
2s	2	.47	0.105
2p	6	.36	0.2
3s	2	4.8	0.93
3p	6	5.42	3.20
3d	10	6.6	6.41

Total $\bar{\Phi}$ for Cu^+ = 10.9 volts.

From equation (6.10):

$$\bar{\Phi} = \frac{e}{4\pi\epsilon} \sum_{ij} N_i E_{ij} A_j$$

In the case of Cu , there is only one type of atom, so that:

$$\bar{\Phi} = \frac{e}{4\pi\epsilon} \sum_{j} E_j A_j N_i$$

$$= \frac{e}{4\pi\epsilon\Delta} \sum_{j} E_j A_j \quad \text{(where } \Delta \text{ is the atomic volume, i.e. } \Delta N_i = 1\text{)}$$

$$= \frac{e}{\pi a_o^3} \sum_{j} E_j A_j \text{ e.s.u.} \quad \text{as } \Delta = a_o^3/4 \text{ for a F.C.C. crystal}$$

$$= .097081 \sum_{j} E_j A_j \text{ volts}$$

For the 3p shell, $E_j = 6$

$$\therefore \quad \bar{\Phi}_{3p} = .097081 \times 6 \times 5.42$$

$$= 3.16 \text{ volts}$$

The $\bar{\Phi}$ values due to the other shells are noted in Table 6.2.

The value of the mean inner potential $\bar{\Phi}$ depends greatly on the outer electrons of the crystal atoms. However, the exact forms of the wave functions for the outermost electrons of an atom in the crystal lattice are not known.

One way of calculating $\bar{\Phi}$ would be to assume the crystal to consist of free neutral atoms. Another extreme way is to take ions at the lattice points, and to assume that the remaining electrons are distributed uniformly. In this present case the copper crystal was assumed to consist of Cu^{+} ions together with an average of one conduction electron per ion. If the conduction electrons are paired with the positive charges of the ions, the contribution of the resulting combination to the inner potential of the crystal has been shown by Bethe (1928b) to be $3e/10R_i$, where R_i is the atomic radius of the crystal. The value of R_i being that which satisfies the volume condition, i.e.

$$\sum N_i \, 4\pi R_i^3/3 = \text{volume of crystal.}$$

Thus the contribution made by the 4s electron is:

$$\bar{\Phi}_{4s} = \frac{3e}{10 \times 1.43 \times 10^{-8}} \text{ e.s.u.}$$

since $R_i = 1.43 \times 10^{-8}$ cm. for copper,

$$= 3 \text{ volts.}$$

Thus the inner potential $\bar{\Phi}$ of copper is $(10.9 + 3) = 13.9$ volts.

6.4 A SIMPLIFIED METHOD FOR THE EVALUATION OF INNER POTENTIAL FROM EQUATION (6.1)

The following simplified method using atomic scattering factors to evaluate the mean inner potential of a crystal is due to Professor M. Blackman.

The evaluation of inner potential in Section 6.3 from equation (6.1) by atomic scattering factors, can be done more simply as follows.

The scattering factor function $F_{nl}(\theta)$ is given by the expression:

$$F_{nl}(\theta) = \int_0^\infty \rho(r) \frac{\sin kr}{kr} \cdot 4\pi r^2 \, dr; \tag{6.11}$$

where: $$k = \frac{4\pi \sin \theta}{\lambda} \tag{6.12}$$

For a sufficiently small Bragg angle θ:

$$\frac{\sin kr}{kr} = \frac{kr - \frac{(kr)^3}{3!}}{kr} = 1 - \frac{1}{6} k^2 r^2 + \ldots$$

and $$F_{nl}(\theta) = \int_0^\infty \rho(r).4\pi r^2 dr - \frac{1}{6} k^2 \int_0^\infty \rho(r).4\pi r^2 \times r^2 dr$$

Taking one electron in a given shell:

$$\int_0^\infty \rho(r) 4\pi r^2 dr = 1$$

$$\therefore \quad F_{nl}(\theta) = 1 - \frac{1}{6} k^2 \overline{r^2}$$

where $$\overline{r^2} = \int_0^\infty r^2 . W(r) dr \Big/ \int_0^\infty W(r) dr$$

$$W(r) = 4\pi r^2 \rho(r), \text{ and } \int_0^\infty W(r) dr = 1.$$

Now $k^2 = \frac{16\pi^2 \sin^2\theta}{\lambda^2}$, and $\frac{\sin\theta}{\lambda} = \frac{1}{2D}$,

where D = Bragg spacing = $\frac{d}{n}$

θ, is Bragg angle.

$$k^2 = \frac{16\pi^2}{4D^2} = \frac{4\pi^2}{D^2}$$

$$F_{nl}(\theta) = 1 - \frac{2\pi^2}{3D^2}\overline{r^2} \qquad (6.13)$$

Pauling's description of F_{nl} as a function of (x^2)

Pauling's expression for $F_{nl}(\theta)$ can be evaluated for small x^2 as:

$$F_{nl} = 1 - f_{nl}x^2 = 1 - f_{nl}\frac{n^2\pi^2 a_o^2}{D^2(Z-S_s)^2} \qquad (6.14)$$

where $x = \frac{n\pi a_o}{D(Z-S_s)}$,

n, is the principal quantum number,

a_o, is the Bohr radius,

S_s, is the screening constant,

and f_{nl} is a numerical constant.

From equations (6.13) and (6.14) we get:

$$\frac{2}{3}\left(\frac{\pi^2}{D^2}\right)\overline{r^2} = f_{nl}\left(\frac{\pi^2}{D^2}\right).\frac{n^2 a_o^2}{(Z-S_s)^2}$$

$$\therefore \quad \overline{r^2} = f_{nl} \times \frac{3}{2} \cdot \frac{n^2 a_o^2}{(Z-S_s)^2}$$

Using the Bethe integral for one electron, then:

$$\Phi_{nl} = \frac{2\pi}{3\Delta} \times e \times 300 \times \overline{r^2} \text{ volts} \qquad (6.14)$$

$$= \frac{2\pi}{3\Delta} \times 300 \times e \times f_{nl} \times \frac{3}{2}\frac{n^2 a_o^2}{(Z-S_s)^2} \qquad (6.15)$$

This $\bar{\Phi}_{nl}$ has to be multiplied by the number of electrons in the (nl) shell. Following this procedure, the inner potential of copper, due to the various shells, has been calculated and is given in Table 6.3.

TABLE 6.3

Electron shell	Number of Electrons	$\bar{\Phi}$ in volts
1s	2	.002
2s	2	.11
2p	6	.215
3s	2	.884
3p	6	2.25
3d	10	6.69
4s	1	3.0*

* directly from Bethe.

$\therefore$ total $\bar{\Phi}$ for Cu = 13.2 volts.

Calculations were carried out for silver, and gold in the same way, which gave the values of 25 volts and 39.9 volts respectively.

6.5 CALCULATION OF INNER POTENTIAL BY USING RECENT HARTREE-FOCK WAVE FUNCTIONS

The value of $\overline{r^2}$ has been computed and published by Charlotte Froese Fischer (1972) using Hartree-Fock wave functions. Using this $\overline{r^2}$ value from Fischer, the inner potential of a crystal may be obtained immediately from equation (6.14). The value of $\bar{\Phi}$ due to the various shells of copper are given in Table 6.4. The potential due to the 4s conduction electron has been calculated,

assuming it to be smeared inside the atomic radius R_i as mentioned in Section 6.3.

TABLE 6.4

Electron shell	Number of Electrons	r^2 in square Bohr units	$\bar{\Phi}$ in volts
1s	2	.003748	.0054
2s	2	.006499	.096
2p	6	.05275	.23
3s	2	.595300	.86
3p	6	.665051	2.87
3d	10	1.104819	7.95
4s	1	Directly from Bethe	3.00

Total $\bar{\Phi}$ for Cu = 15.00 volts.

Similar calculations were carried out for silver and gold, giving 18.9 volts and 25.5 volts, respectively.

6.6 INNER POTENTIAL OF DIAMOND

Using Bethe's formula (equation 6.1) and the numerical Hartree-Fock-Slater atomic radial wave functions by Hermann and Skillman (1963), Radi (1970) obtained 15.93 volts for diamond. In this calculation the outermost 2p electrons were assumed to be smeared uniformly inside the atomic volume (see Chapter 7, Section 7.3).

6.7 THE CALCULATED VALUES OF INNER POTENTIAL OF SODIUM CHLORIDE, POTASSIUM BROMIDE, CALCIUM FLUORIDE AND SILICON

Theoretical calculations for the substances sodium chloride, potassium bromide, calcium fluoride and silicon mentioned in Chapter 5, Section 5.10, are summarized in the following Table 6.5.

TABLE 6.5

Calculations by	Φ in volts for				Method used
	NaCl	KBr	CaF_2	Si	
1) Miyake (1940)	7.1-7.9	-	7.3-8.8	-	Diamagnetic susceptibility
2) Tull (1951a)	8.7	-	-	-	Atomic scattering factor and Pauling's function
3) Kehoe (1956)	7.17	7.3	-	-	Diamagnetic susceptibility
4) Bühner and Sleeb (1967)	7.33	8.32	-	-	Using approximations to X-ray scattering factors from improved wave functions
5) Radi (1970)	9.54*	9.57*	-	11.5	Hartree-Fock-Slater wave functions

* It is not clear what wave functions were used by Radi (1970) for sodium chloride and potassium bromide.

CHAPTER 7

SUMMARY AND COMMENTS

7.1 GENERAL

There are considerable differences between several of the inner potential measurements made by other workers and those presented here. Furthermore, there are appreciable discrepancies to be found among previous results for similar substances (see Tables 1.1 and 5.12). These differences will be discussed, as far as possible, in the following.

7.2 EXPERIMENTAL

7.2.1 Silver and Gold

Tull (1951a) measured the inner potential of silver and gold by Yamaguti's method and obtained 23.3 $\pm$ 1.0 volts and 30.2 $\pm$ 0.9 volts, respectively. These are about 25% higher than those of the present work. It is difficult to account for these differences and because of this a number of other substances were measured as a check (Chapter 5, Section 5.10). No other previous experimental work indicates a value as high as that obtained by Tull for gold. Other values for gold (see Table 1.1), all determined by the electron interferometric method, compare reasonably well with that of the present work, except that of Kerschbaumer (1967), who obtained 16.8 $\pm$ 1.0 volts - a value barely greater than a half of that obtained by Tull.

Yoshida (1954) made measurements on the inner potential of silver using a reflection method and obtained 22.0 $\pm$ 6.0 volts.

Yoshida's average value for silver is about 4 volts higher than that of the present work. However, because of the nature of the method used, Yoshida's results are not likely to be very accurate (see Appendix 3).

Buhl (1959) using the electron interferometric method obtained the inner potential of silver and gold as 20.7 $\pm$ 0.7 volts, and 21.2 $\pm$ 2.0 volts, respectively. Buhl's value for silver is about 3 volts higher than the present one, but his average value for gold agrees fairly well with that of this work. Keller (1961) using the same method, obtained 17-21.8 volts and 22.1-27 volts for silver and gold, respectively. The present experimental value for silver, 17.7 $\pm$ 0.9 volts (see Table 5.12), agrees fairly well with Keller's, but his result for gold is a few volts higher. As already mentioned, Kerschbaumer obtained 16.8 $\pm$ 1 volts for gold, which is about 5 volts lower than the present value. An examination of Kerschbaumer's detailed results seems to show that the inner potential value for gold tends to increase with increase of specimen thickness. It is possible that the density of the specimens is less than that for the bulk material, which might result in a lower value for the inner potential.

The variation in the results obtained using the electron interferometric methods may possibly be due to inaccuracies in measuring the film thickness. It is worth noting that the accuracy of the method depends to a great extent on the measurement of the thickness of the specimens used. According to Rymer (1970), the inner potential of a crystal, using this method, cannot be measured more accurately than about $\pm$15% due to the difficulty of measuring the specimen thickness.

7.2.2 Copper

Yoshida (1954) made measurements on the inner potential of copper using a reflection method and obtained 8-14 volts which, on average, is lower than that obtained from the present work. As already mentioned (see Section 7.2.1 and Appendix 3), Yoshida's results are not likely to be very accurate. Steeb and Bühner (1967a) used the reflection method on electropolished specimens of copper, the diffraction patterns from which showed streaked spots indicating good flat surfaces. The wavelength was measured by means of a calibration experiment. (100) and (111) surfaces were prepared, both giving 19 volts. No explanation has yet been found to account for the difference between this (higher) value and the present one.

Using the interferometric method, Keller (1961) obtained for copper 23.5 $\pm$ 0.6 volts, which is about 40% higher than the present value (see Table 5.12). It is striking to note that for Keller's result the inner potential of copper is significantly higher than his values for silver and gold. According to the recent theoretical calculations of Radi (1970), copper would be expected to have an inner potential less than that of silver and gold. Due to the high reactivity of copper with oxygen, it is possible that an oxide layer is formed on the specimen surface which might affect the result, but no real evidence has in fact been found to account for the differences. Hoffmann and Jönson (1965) obtained 20.0 $\pm$ 1.0 volts, which again is about 6 volts higher than that of the present work but about 15% lower than Keller's value. It is difficult to account for the difference between Keller's and Hoffmann and Jönson's result, since the same measuring method has been used in both cases. Again no explanation has been found to account for the 6 volts disparity between Hoffmann

and Jönson's measurement and that of the present work. Kerschbaumer (1967) obtained 20.2 ± 0.7 volts, which is in good agreement with Hoffmann and Jönson but this also is higher than his results for gold.

7.2.3 Diamond

Beeching (1940) measured the inner potential of diamond by Yamaguti's and by Shinohara's method and obtained a mean value of 20.8 ± 0.7 volts. This is about 6 volts higher than that of the present work. It is not clear why his result is so high, but it is likely that he made use of relatively few orders of reflection.

Schwarzer et al. (1975) measured the inner potential of diamond by two methods using horizontal Kikuchi lines. The first method is a direct one, similar to that of Shinohara, in which the position of the shadow edge has to be determined accurately (see Chapter 2, Section 2.3). The second is a "fitting" procedure which does not involve the shadow edge. In this case only the distances between lines need to be measured, the final result involving a fitting of the inner potential to the known accelerating voltage. The methods gave substantially the same result, the average value being 18.6 ± 2.2 volts. It is some 3 volts higher than that of the present work. It should be noted here that measurements based on horizontal Kikuchi lines in the present work gave an average result of 17.3 ± 1.5 volts, which is also higher than that obtained by the Yamaguti method.

The accuracy of Shinohara's method depends on locating the position of the shadow edge accurately. In the present work this has

been done by following the procedure given in Chapter 2, Section 2.3. This method appears not to have been used previously. It depends on the precision with which a given Bragg spot can be made to coincide with the corresponding horizontal Kikuchi line. (If the two positions differ by about .05 mm., a not unreasonable amount, the corresponding error in calculating the inner potential should be only about $\pm$ 0.2 volts.)

Finally, the measurements made on the additional substances as a check also show some unaccountable discrepancies. Thus the present measurements made on sodium chloride and potassium bromide agree well with those of Kehoe (1957) but are about 25% lower than the values obtained by Tull (1951a) for sodium chloride and by Bühner and Steeb (1967a) for sodium chloride and potassium bromide. The present results for silicon and calcium fluoride appear to be in good agreement with past work (see Table 5.13).

7.3 COMMENTS ON THE THEORETICAL CALCULATIONS

Previous theoretical calculations are summarized in Chapter 1, Table 1.2. The most recent and comprehensive of these is due to Radi (1970), who calculated the inner potentials of copper, silver and gold by using recently published Hartree-Fock-Slater atomic radial functions by Herman and Skillmann (1963). For each element he gives a "high" and a "low" value. The high values are obtained by assuming that the crystal consists of free neutral atoms. The low values are obtained by adding the potential of the p times ionized free atom (i.e. the p outermost electrons of the neutral atom are missing; in the case of copper, silver and gold p = 1), with the

potential of the p free electrons which are assumed to be smeared uniformly inside the atomic volume (see Bethe 1928b) as discussed in Chapter 6, Section 6.3. The low values of Radi's calculation are likely to be more accurate representations in the crystalline state. Radi's low values for copper, silver and gold are 15.8 volts, 18.7 volts and 25.0 volts, respectively, and are in fair agreement with the present experimental results. Calculations for the present work were also carried out using the Hartree-Fock wave functions prepared by Charlotte Froese Fischer (1972) (see Chapter 6, Section 6.5); these gave very similar values for copper, silver and gold, being 15.0 volts, 18.9 volts and 25.5 volts, respectively. Here also, the single outermost electron was considered to be smeared uniformly inside the atomic volume.

For diamond, Radi gives two theoretical values for the inner potential. The first is based on the carbon atom and also uses the Hartree-Fock wave functions of Hermann and Skillmann, yielding a value of 19.75 volts. For the second value he uses a method appropriate to metals in that the outer four electrons are assigned a constant density over the atomic volume. This gives 15.93 volts, but it is very doubtful whether this procedure, which is suitable for metals, is in any way appropriate to diamond.

It is evident that, for a given crystalline substance, measurements of the inner potential made by different experimentalists, in many cases, differ widely one from another. These differences, which are sometimes as great as 25% and often well outside the experimental errors quoted, usually about 15%, emphasize the need for a detailed and critical analysis of a series of experiments preferably carried out in more than one laboratory. The theory of the present Yamaguti and Shinohara methods assumes the kinematic diffraction theory modified by the effect of refraction. It would be highly desirable to carry out a multi-ray calculation to construct the intensity curves appropriate to the reflection methods.

APPENDIX 1

RELATION BETWEEN THE INNER POTENTIAL Φ, AND REFRACTIVE INDEX μ OF A CRYSTAL

According to De-Broglie, a particle, for example an electron, having momentum p can be represented by a wave of wavelength λ, where:

$$\lambda = \frac{h}{p} \tag{A1.1}$$

and h is Planck's constant. Suppose an electron, initially at rest at a point where the electrostatic potential is zero, moves to a point where the potential is P. Then equating the reduction in potential energy to the gain in kinetic energy,

$$Pe = \frac{p^2}{2m} \tag{A1.2}$$

where e and m are the charge and mass of the electron respectively. Eliminating p from equations (A1.1) and (A1.2):

$$\lambda = \frac{h}{\sqrt{2meP}} \tag{A1.3}$$

Due to the presence of the (positive) inner potential, Φ, electrons entering or leaving a crystal experience a change in wavelength and will be refracted. If P is the accelerating potential, the kinetic energy of the electrons will be eP outside the crystal and $e(P + \Phi)$ inside. The ratio of the wavelength, λ_o, for electrons travelling in vacuum to the wavelength, λ_i, for electrons travelling inside the crystal defines a refractive index, μ, i.e.

$$\mu = \frac{\lambda_o}{\lambda_i}$$

$$= \left[\frac{P + \Phi}{P}\right]^{\frac{1}{2}} \qquad \text{(from equation (A1.3)}$$

$$\therefore \quad \mu^2 = 1 + \frac{\Phi}{P}$$

APPENDIX 2

WAVELENGTH AND CAMERA LENGTH CONSIDERATION

PART A

The expression for the refractive index μ of a crystal is given by:

$$\mu^2 - 1 = \frac{n^2 \lambda_o^2}{4d^2} - \sin^2 \beta_n \qquad \text{(see equation (2.4) of Chapter 2)}$$

where n, λ_o, d and β_n have their usual meanings.

If the correct wavelength λ_o is used, the points obtained by plotting $(\mu_n^2 - 1)$ for different orders n, against n^2, should lie on a line parallel to the n^2 axis so that $(\mu_n^2 - 1)$ will be constant, i.e. $(\mu^2 - 1)$. Since, in general, λ_o' differs from the true wavelength, λ_o, $(\mu_n^2 - 1)$ will vary with n^2 and plotting these two quantities will, therefore, result in a straight line of non-zero slope. Nevertheless, irrespective of the magnitude of λ_o', all such lines should intersect the $(\mu_n^2 - 1)$ axis in the same point, i.e. at $(\mu^2 - 1)$ (see Fig. 2.4, Chapter 2).

In order to check this, calculations have been carried out with different λ_o' values and $(\mu^2 - 1)$ values are obtained for each of them. These are summarized in Table A2.1.

TABLE A2.1

L = 25.23 cm.

Approximate accelerating potential = 45 kV

Approximate wavelength $\lambda_o' A^o$	Correct wavelength λ_o A^o	$(\lambda_o' \sim \lambda_o)$ in A^o	$(\mu^2-1)\times10^5$	$\mathfrak{V}$, in volts
1) .055	.05787646	.0031388	37.6747	15.6
2) .057	.05787634	.0008763	37.6703	15.6
3) .058	.05787660	.0001234	37.6814	15.6
4) .059	.05787636	.0011236	37.6738	15.6
5) .061	.05787653	.00312347	37.6761	15.6

The results of Table A2.1 are represented in Fig. A2.1.

From the above results it is clear that the value of inner potential calculated does not depend on the value of the approximate wavelength λ_o' chosen at the outset.

PART B

In the present work, the perpendicular distance between the centre of the specimen holder and the photographic plate is 25.23 cm. It is possible for a given specimen for the camera length to differ a little from this, as indicated below.

(I) The size of specimens used was usually rather less than about one centimetre square. Thus the camera length, i.e. the distance between the point of incidence of the electrons on the surface of the crystal and the photographic plate could differ by about ± 5 mm. (see Fig. 3.1, Chapter 3). Calculations have been carried out for a particular Yamaguti-type measurement of diamond (111) by assuming that the camera length varied in increments from 24.5 cm. to 25.5 cm. The corresponding inner potential values were found to vary from 15 volts to 15.9 volts and these are displayed in the Table A2.2 following.

TABLE A2.2

$\lambda_o' = .058\ A^o$

L cm.	(corrected) A^o	$(\lambda_o' - \lambda_o)\ A^o$	$(\mu^2-1) \times 10^5$	$\mathcal{V}$, in volts
24.50	.0594842	-0.001484	38.14	15.01
24.75	.0589240	-0.000924	37.99	15.2
25.00	.0583640	-0.000364	37.38	15.2
25.23	.0578766	+0.0001234	37.68	15.6
25.50	.0573060	+0.000694	37.62	15.9

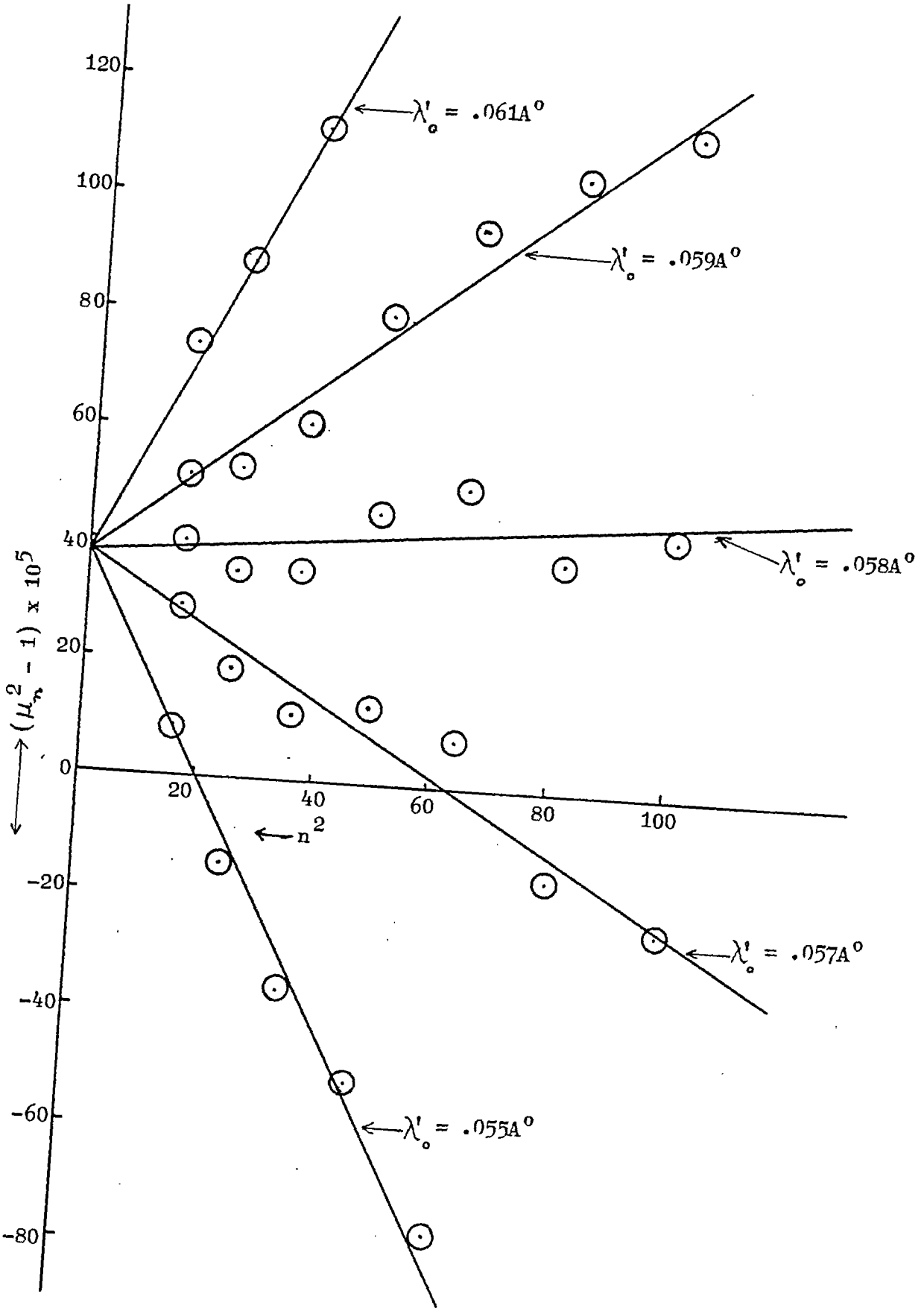

120
100
80
60
40
20
0
-20
-40
-60
-80
20
40
60
80
100
n^2
$(\mu_n^2 - 1) \times 10^5$
$\lambda'_o = .061A^o$
$\lambda'_o = .059A^o$
$\lambda'_o = .058A^o$
$\lambda'_o = .057A^o$
$\lambda'_o = .055A^o$

FIG. A2.1

(II) Ideally, the specimen should be positioned as shown in Fig. A2.2(a), the axis of rotation coinciding with the point of incidence of the electron beam. However, it is possible that the specimen may sometimes be situated in a position such as that shown in Figs. A2.2(b) or A2.2(c). It is evident in the latter two cases that as the specimen is rotated, the camera length L will vary slightly from order to order. From the considerations of the geometry and taking the largest value of d likely to be encountered as 3 mm., the maximum error from the above source is estimated to be about ± 0.5 volts.

It is also estimated that the combined errors from (I) and (II) could amount to about ± 1.0 volts.

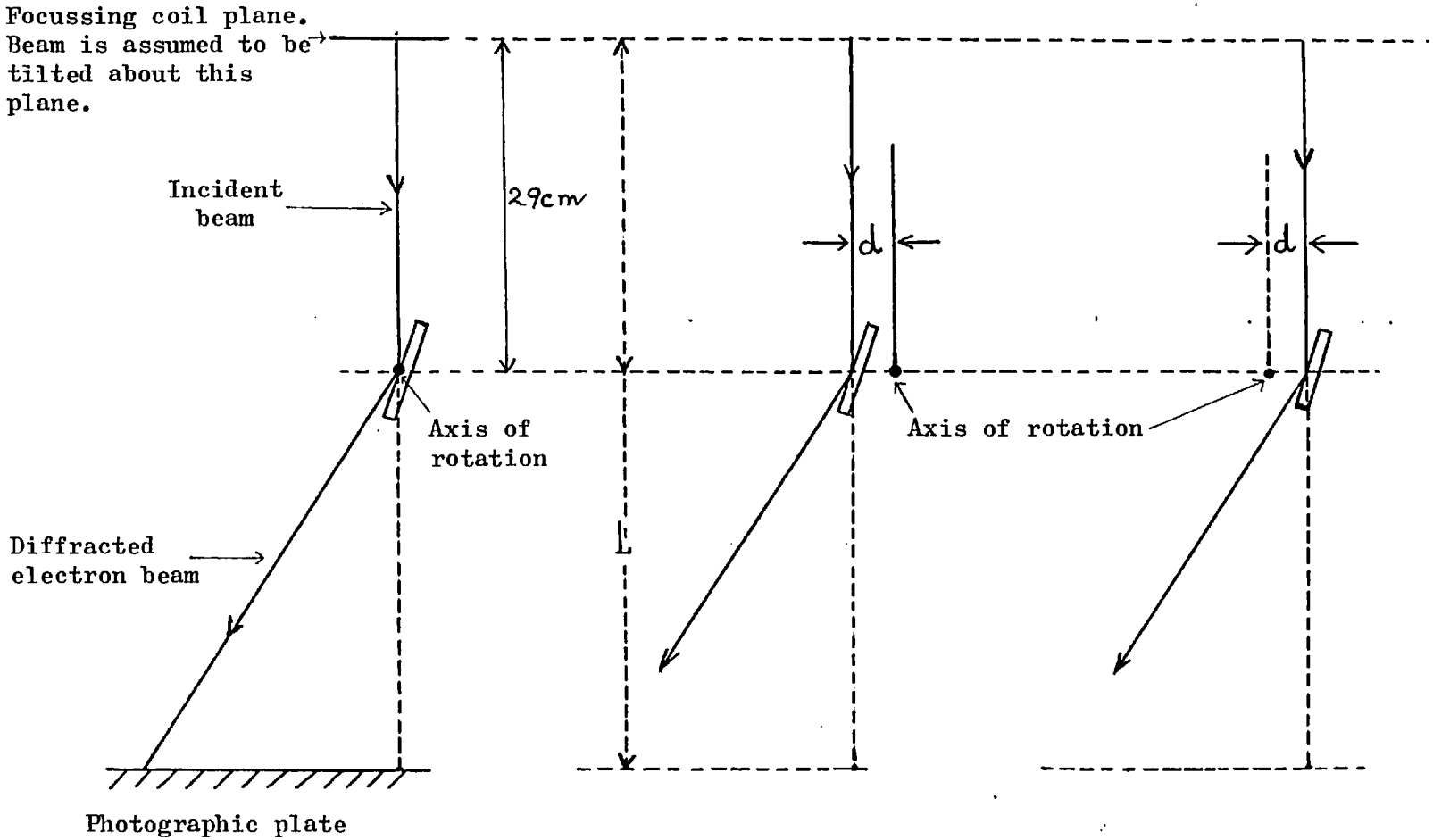


FIG. A2.2(a)

FIG. A2.2(b)

FIG. A2.2(c)

APPENDIX 3

YOSHIDA'S (1954) METHOD FOR MEASURING INNER POTENTIAL

This is based on the examination of small facets which appear on the surface of electropolished metal single crystals (see Fig. A3.1). Yoshida measured the total deviation Δ_n between the incident and diffracted electrons. It can be shown that:

$$\Delta_n = 2(\psi'_n - \psi_n) = \frac{\phi}{E} \cdot \frac{1}{\delta + \theta_n}$$

where ϕ is the inner potential, E is the accelerating potential, θ_n is the Bragg angle for the n^{th} order reflection, and the symbols ψ'_n and ψ_n are as shown in Fig. A3.1.

The accuracy depends not only on the precision to which the accelerating voltage E is measured, but also on the angle δ. Furthermore, the section of the facet shown diagrammatically in Fig. A3.1 is assumed to be an isosceles triangle, the beam supposedly entering one sloping face and leaving the other. It is further assumed that the macroscopic surface is exactly parallel to the net planes. There is no real evidence presented to support any of these assumptions and furthermore, according to Yoshida himself, the angle δ cannot be found with precision. It would appear that Yoshida's results can be regarded only as uncertain approximations.

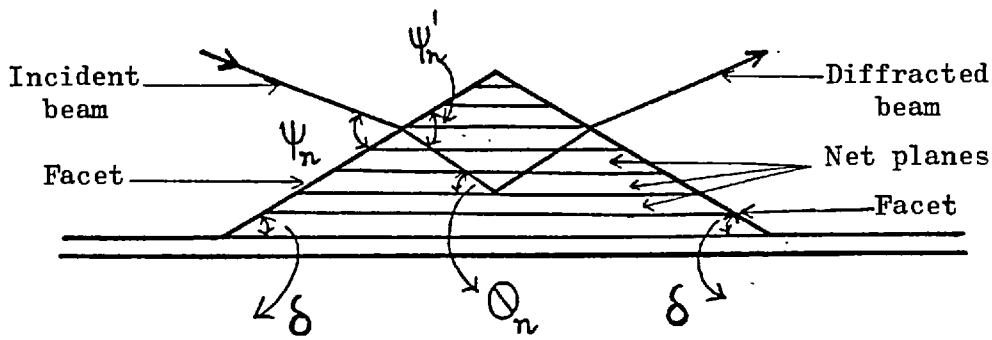

Incident beam
Facet
ψ_n'
ψ_n
Diffracted beam
Net planes
Facet
δ
θ_n
δ

FIG. A3.1

ACKNOWLEDGEMENTS

The author wishes to express her deep gratitude to Dr. N.D. Lisgarten for suggesting the original problem, for providing the necessary facilities and for giving constant help and encouragement during the course of this work, which was carried out under his supervision.

The author's thanks are due to Professor M. Blackman for many helpful discussions regarding the theoretical aspects and to Dr. P. Dobson, Dr. Gregory Burland and Geoff Spiller for general help.

The author is indebted to the Government of India for a scholarship, and to her parents for their unfailing encouragement.

REFERENCES

Anishehenko, R.I. (1966), Phys. Stat. Sol. 18, 923.

Bearden, J.A. (1927), Phys. Rev. 29, 29.

Beeching, R. (1935), Phil. Mag. 20, 841.

Bethe, H. (1927), Naturwiss. 15, 786.

Bethe, H. (1928a), Naturwiss. 16, 333.

Bethe, H. (1928b), Ann. d. Phys. 87, 55.

Brill, Grimm, Hermann et al. (1939), Ann. d. Phys. 34, 393.

Buhl, R. (1959), Zeit. für Physik 155, 395.

Davisson, C.J. and Germer, L.H. (1927), Nature 119, 558.

Fischer, C.F. (1972), Atomic data, 4 (4), 309.

Fuchs, K. (1935), Proc. Roy. Soc. London A151, 585.

Hartree, D.R. (1932), Proc. Roy. Soc. London A141, 282.

Hartree, D.R. (1935), Proc. Roy. Soc. London A151, 96.

Hermann and Skillmann (1963), Atomic structure calculations, Englewood Cliffs: Prentice Hall.

Hoffmann, H. and C. Jonsson (1965), Zeit. für Physik 182, 360.

Kehoe, R.B. (1957), Phil. Mag. 2, 455.
(1956), Ph.D. Thesis, London.

Keller, M. (1961), Z. Physik 164, 274.

Kerschbaumer, E. (1967), Zeit. für Physik 201, 200.

Kozlenkov, A.I. (1963), Bull. Acad, Science U.S.S.R. Physics Science 27, 378.

Menadue, J.F. (1972), Acta Cryst. A28, 1.

Miyake, S. (1940), Proc. Phys. Math. Soc. Japan 22 Part 8, 666.

Mollenstedt, G. and Düker, H. (1956), Z. Phys. 145, 377.

Pauling, L. and Sherman, J. (1932), Z. f. Cryst. 81, 1.

Pinsker, Z.G. (1953), Electron diffraction, London: Butterworths, p. 139.

Radi, G. (1970), Acta Cryst . A26 Part 6, 41.

Rymer, T.B. (1970), Electron diffraction, London: Methuen & Co. Ltd.

Schwarzer, R.A. et al. (1971), Optik 33, 215.

Schwarzer, R.A. et al. (1975), Optik 44 (1), 37.

Shinohara, K. (1932a), Sci. Pap. I.P.C.R. Tokyo 18, 223.

Shinohara, K. (1932b), Sci. Pap. I.P.C.R. Tokyo 18, 315.

Siota, Y. (1958), The science reports of Tohoku University, First series, XL11N04, 173.

Steeb, S. and Bühner, H.F. (1967a), Z. Naturforsch. 22a (12), 1990.

Steeb, S. and Bühner, H.F. (1967b), Z. Naturforsch. 22a (12), 1994.

Thomson, G.P. and Cochrane, W. (1939) Theory and Practice of Electron Diffraction, London: Macmillan & Co. Ltd., Chapters X and XVIII.

Tillman , J.R. (1934), Phil. Mag. 18, 656.

Tull, V.F.G. (1951a), Proc. Roy. Soc. London A206, 219.

Tull, V.F.G. (1951b), Proc. Roy. Soc. London A206, 232.

Veldkamp, J. (1933), Zeit. für Physik 82, 776.

Wyckoff, R.W.G. (1974) Crystal Structure, London: Interscience Publishers.

Yamaguti, T. (1930), Proc. Phys. Math. Soc. Japan, 12, 203.

Yamaguti, T. (1932), Proc. Phys. Math. Soc. Japan 14, 57.

Yoshida, S. (1954), Acta Cryst. 7, 592.